# Vision - Based Navigation for Moon Landing

*Final Report for ESTEC purchase order 142958*


Contributing authors:

Gerhard PAAR
Michael ULM
Oliver SIDLA

ESTEC Technical Managers:
Patrick PLANCKE
Jean de LAFONTAINE

Graz, December 1994

*Issue 1*

*Contact Address:*
*Gerhard Paar*
*JOANNEUM RESEARCH*
*Wastiangasse 6*
*A - 8010 Graz*
*AUSTRIA*
*Tel. +43 316/876-716*
*Fax +43 316/876-720*
*email paar@pdib40.joanneum.ac.at*

# 1 INTRODUCTION AND SCOPE

The European Space Agency is currently considering a four-phase Moon Exploration Program, beginning with initial unmanned lunar resource exploration and a first launch in the beginning of the 21st century.
In the framework of the Lunar European Demonstration Approach (LEDA) mission, this study deals with ground-based on-board intelligent processing of sensor data to allow the reconstruction of a region of interest and the selection of a safe landing site from orbital data as well as real-time navigation of the spacecraft during descent until hazard-free landing.
Recent and ongoing Theme-4 activities [[Mat93]], [[PPC92]], [[PSC+94]] cover planetary mission navigation in terms of Mars and Comet scenarios. Adaptation of the existing methods for application in a Moon landing scenario in terms of parametric input to the procedures is one task of this study. Its main objectives are to point out the technical requirements, limitations, functionality and expected performance of a computer vision system that supports a safe and accurate landing, taken into account the environmental and mission background. This includes the realistic extraction of those strategies that are explicit proposals for sensing computational methods in the framework of a whole orbiter/landing scenario.

Sections 2 to 7 are dedicated to the definition of several strategies accounting for different realistic landing scenarios. Section 8 describes a hardware solution. Section 9 deals with a detailed analysis of the strategies in terms of performance, requirements, and system impacts. Some theoretical aspects of the accuracy estimations are shown in Appendix A.
The strategies and results are summarized in Section 12.

Major results of this study are illustrated in a video available at JOANNEUM RESEARCH or ESTEC (Patrick Plancke, WDP).

# 2 DEFINITION OF STRATEGIES

## 2.1 Terminology

A "strategy" is defined as the set of measurements, processing, spacecraft maneuvers and operations carried out by the ground and space segments during the orbital and descent/landing phases in order to meet the requirements to the navigation-vision system.
Beginning with Section 3.1, strategy components (SC*n*) are described that can be combined to whole strategies.

## 2.2 Strategy Description Format

The description of a strategy contains all relevant information that allows its analysis and, in a further step, the evaluation of its relevance for a realistic mission. In the following the used descriptors are listed. For important parameters, their lower and upper bounds and the influence of deviation between these values to the performance and requirements are given as well.

- Trajectory Profile + image acquisition times
- Prerequisites in terms of prior strategy components
- Limitations from the environment
- In particular: Influence of illumination/time of day (within the given borders)
- Drawbacks from surface morphology and texture
- Required processing components (overview)
- Results and benefits of this strategy for the complete mission
- List of required "external" sensors
- Required experiments (described in Section 9)
- Parameter tables that are relevant, both coming from theoretical considerations and experiments
- Relevance from a realistic point of view
- Expected performance (to be compared with experimentation results) and applicability

The expected computational performance (update rate and memory requirements) is listed in Section 8.

## 2.3 Target Mission Scenario

Table 1 gives details about the reference parameters in terms of mission and environment. Landing site is near the south pole at a latitude of more than 82°. Target region is the rim of a large crater that is still illuminated. The region should be flat, the touch-down point should allow the deployment of a small rover probably into the crater. A polar orbit is assumed with about 100 km ground distance and approx. 2 hours period.

| Schedule | |
|---|---|
| Launch | 2001 |
| Days in orbit | < 30 |
| **Orbit** | |
| Orbit orientation | Polar |
| Orbit height | 100 km |
| Orbit height above landing site (last orbit) | 15 - 25 km |
| Circulation period | 2 h |
| Velocity relative to landing site | 1.7 km/sec |
| **Landing Site** | |
| Location | > 82° latitude at south pole |
| Morphology | Crater Rim |
| Illumination | Daylight (dark inside crater) |
| Sun angle | 3-13 ° |
| Approach direction | from near *or* far side |
| **Landing** | |
| Horizontal entry accuracy along track | < 3 km |
| Horizontal entry accuracy across track | < 1 km (TBC) |
| Vertical entry accuracy | < 300 m |
| Descent velocity | 10 - 20 m sec |
| Entry elevation (hor. vel. = 0) | 5 km |
| Descent duration | 250 sec |
| Roll angle accuracy (around x,y) | < 2° |
| Tilt angle accuracy (around z) | < 5°(TBC) |
| Thruster stopping altitude (v(vert) = 0) | 30 m |
| Touch-down speed | 10 m/sec |
| Free fall time | 6.5 sec |
| **Landing Area/Spot** | |
| Size | 5 km diameter |
| Size of landing spot | 5 m diameter |
| Maximum slope at landing spot | 20° |
| Maximum obstacle size at landing spot | 0.5 m |
| **Vision System Requirements** | |
| Beginning of navigation | 5 km ground distance |
| Navigation accuracy | 10 m |
| Hazard detection | 0.5 m |
| Update rate | Around 10 sec |

*Table 1: Reference Mission Scenario*

Some important additional parameters (sensor characteristics, pointing accuracy etc.) are listed in Table 2. They serve as baseline used for explicit scenario parameters.

| Transmission | |
|---|---|
| Data rate: Orbiter Earth | 500 kbps |
| **Pointing Accuracy** | |
| Orbiter Camera | 0.02° |
| **Radar Altimeter** | |
| Beam Width | 0.4° |
| Update Rate | 1 Hz |
| | 1 % of range, 5m bias |
| Accuracy | 10 E-7 m/sec2 |
| **Laser Mapper** | |
| Pointing Accuracy | 0.05° |
| Mapping Accuracy | 5m (bias and random) |
| Beam Footprint (at 5 km) | 20 cm |
| Field of View | 8° |
| Map update period (100 x 100 pix) | 200 sec |

*Table 2: Additional mission sensing parameters*

# 3 MAPPING

## 3.1 SC1 Mapping from Orbit Shortly Before Landing

### *3.1.1 SC1 Mission Profile Description*

At most one overfly of the landing area during orbit is foreseen. This implies that the landing area mapping from the orbiter can only be performed during the last orbits before descent. Table 3 lists the relevant parameters for that scenario, the geometric relations are displayed in Figure 1.

| | |
|---|---|
| Moon Elongation change during one orbit (2h) | 1° |
| Resulting horizontal distance between 2 orbits at 82° | 4.5 km |
| viewing angle (to vertical) at last orbit (25 km ground dist) | 10° |
| viewing angle at 2 orbits before descent | 20° |
| viewing angle at 3 orbits before descent | 28° |
| viewing angle at 4 orbits before descent | 36° |
| Size of landing area to be mapped | 6 km x 1.5 km |
| Shadow length vs. obstacle height (10° sun angle) | 6 x obstacle height |
| Ground speed | 1.7 km/sec |

*Table 3: Relevant mission parameters of SC1*

According to Table 3, it is possible to generate stereo views of the landing area with a viewing angle of 36° to vertical already 4 orbits (8 hours) before descent. Depending on downlink capacity, compression rate and required image resolution, this would enable to generate a DEM and ortho image (grey-level image with same x/y geometry as DEM) on ground and select a landing site during the last 3 orbits. Assuming a sensor designed for this task, Table 4 gives parameters of the sensing scenario.

| | |
|---|---|
| **CCD Pixel Size** | **1000 x 1000** |
| **Ground Resolution** | **1.5 m** |
| **DEM Accuracy** | **3 m (TBC)** |
| **Focal Length** | **approx. 200 mm** |
| **Field of View (FOV)** | **1.5km x 6 km** |
| **Number of Images (20 % Overlap)** | **5 x 2** |
| **Required Pointing Accuracy (< 10 % FOV Loss)** | **0.34 deg (6 mrad)** |
| **Pointing Degrees-of-Freedom (DOF)** | **2 (around x and y)** |
| **Required Pointing Velocity** | **> 2 deg/sec** |
| **Left Image Acquisition at (sec)** | **0/0.8/1.6/2.4/3.2** |
| **Right Image Acquisition at (sec)** | **8/8.8/9.6/10.4/11.2** |
| **Image Data Amount** | **10 Mbytes** |
| **Required Transmission Data Rate for Ground Processing** | **10 Kbits/sec** |

*Table 4: Vision sensing parameters of SC1 (example)*

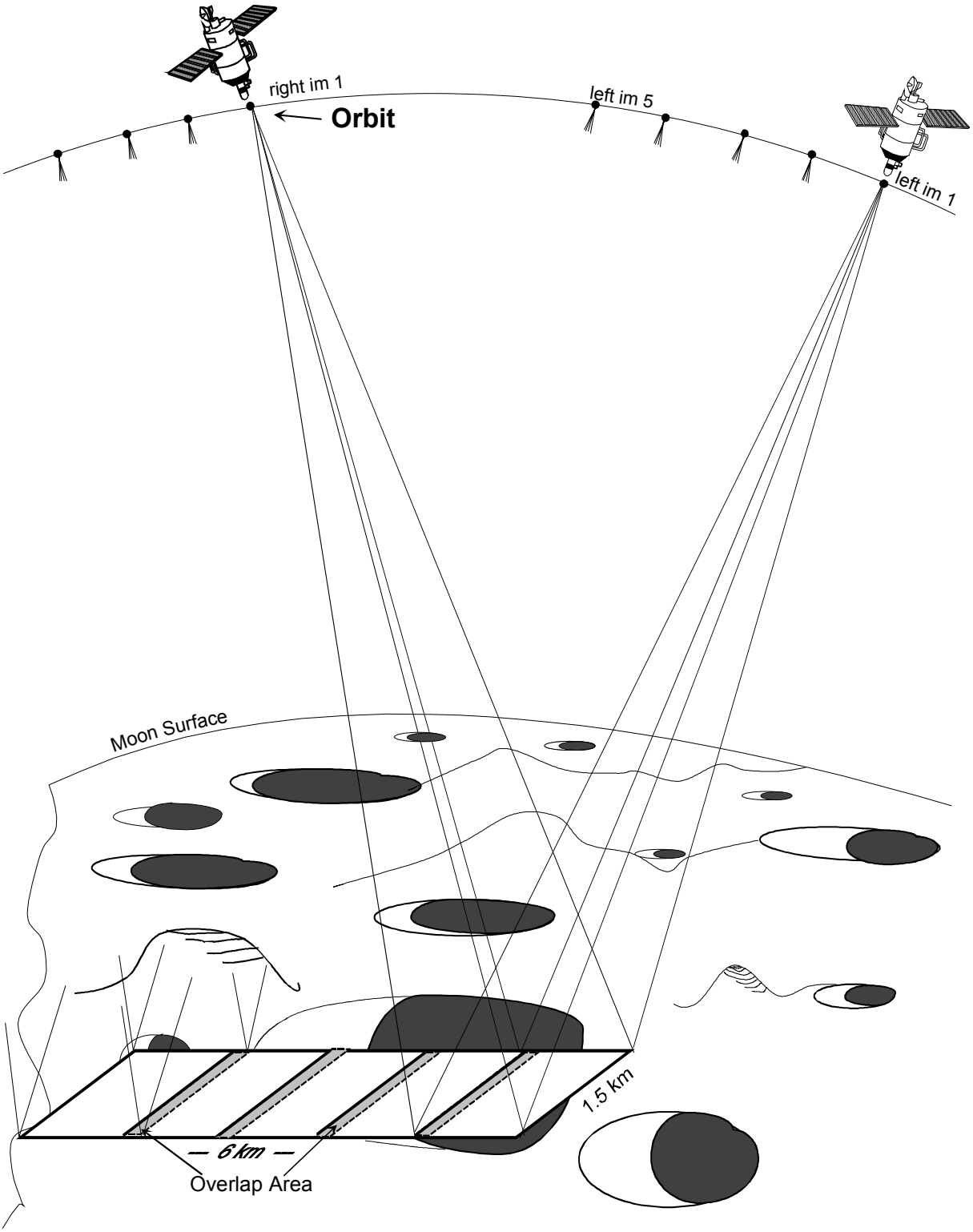


*Figure 1: Geometric scenario of SC1*

### *3.1.2 SC1 Requirements and Limitations (mission/environment)*

1. In principle, the flat illumination induces the appearance of proper texture for stereo matching. Large shadow areas behind hills and inside craters cannot be reconstructed at all, since the contrast is too high to obtain reasonable sensor response in those areas. The elevation map therefore will be sparse. In particular,

the area around a possible landing site can only be reconstructed if it is not located within a shadow. A sparse elevation map might complicate the interactive landing site selection on ground, as well as the image comparison for position initialization.

2. If the landing site is planned on a crater rim, a large area at one side of the rim may be shadowed resulting in a loss of information about the elevations therein.
3. Table 4 shows the necessity to change the pointing direction of the camera by 30 degrees within 8 seconds. This might not be possible if only one fixed camera is available on the orbiter. A solution would be mounting two cameras pointing in the required directions, or a mechanical pointing device with one degree of freedom.
4. There are two possibilities for accurate calibration of the position and pointing parameters:
    a) The orbit is accurately known, the distance traveled between the image acquisition moments must be known preferably better than a meter. Calibration methods are available, that use the stereo disparities together with the distance between the image acquisition points to calculate a consistent stereo calibration.
    b) Reference points are known on the surface for straightforward calibration.

    Since the latter requires interactive actions (identification of the reference points in the orbiter images) and a reaction must be performed within one or two hours if the DEM and ortho image is to be used during landing, the first possibility is to be preferred.

### *3.1.3 SC1 Sensing/Processing Components*

- One CCD array SAC with horizontal FOV in the range of the EU width (example in Table 4; Table 5 gives four different sensing options that will be referred to in all following performance estimations). Since the horizontal velocity is rather high, a non-interlaced sensor array is to be preferred. Optionally, the use of a line scanner array may be considered. Disadvantage is higher complexity of the calibration methods and stronger requirements to the knowledge about orbit dynamics. Advantage of a line scanner is the fact that it is standard space qualified technology even in high resolutions.
- 10 MB storage (1.5 MB second data link required between frame grabber and memory)
- Compression Hardware Data link to ground station (10 Kbits second minimum)

### *3.1.4 SC1 Relevance, drawbacks and benefits*

The access to a high resolution DEM from orbit is one of the most important requirements of many following tasks, both during descent, landing and rover operations. It is therefore strongly recommended to acquire high resolution stereo orbiter images of the landing site surrounding, even if the images are processed after touch-down.

Since it is foreseen to operate the orbiter for some days on a regular orbit, the SAC planned for landing site mapping can be used to map other regions of the moon surface. Considering a data rate of 500 Kbits/second and 20 days of operation, an area of about 30.000 km² (partitioned in separated stripes) could be mapped with 6 m resolution.

### *3.1.5 SC1 Relevant Parameters and Experiments*

The investigations concerning relevant parameters for SC1 will use four different reference scenarios. Table 5 describes these scenarios in terms of sensing. The mission parameters of Table 1 are used therefor.

Option A uses a medium angle camera that can be used for navigation during landing, and hazard avoidance. Its footprint at a distance of 1 km is 125 x 125 m.

| | A | B | C | D |
|---|---|---|---|---|
| N. of CCD Pixels | 512 x 512 | 1024 x 1024 | 512 x 512 | 1024 x 1024 |
| Focal Length | 40 mm | 150 mm | 100 mm | 200 mm |
| Ground Distance | 15 km | 15 km | 25 km | 25 km |
| N. of Images | 3 x 2 | 6 x 2 | 5 x 2 | 5 x 2 |
| **Orbit N (Last before Descent, 4.5 km Horizontal Displacement)** | | | | |
| Target Distance | 15.911 m | 15.911 m | 25.831 m | 25.831 m |
| Footprint | 2037 m | 1086 m | 1323 m | 1292 m |
| Ground Resolution | 3,978 m | 1,061 m | 2,583 m | 1,292 m |
| **Orbit N-1 (9 km Horizontal Displacement)** | | | | |
| Target Distance | 17.718 m | 17.718 m | 26.981m | 26.981 m |
| Footprint | 2268 m | 1210 m | 1381 m | 1381 m |
| Ground Resolution | 4,430 m | 1,181 m | 2,698 m | 1,349 m |
| **Orbit N-2 (13.5 km Horizontal Displacement)** | | | | |
| Target Distance | 20.375 m | 20.375 m | 28.796 m | 28.796 m |
| Footprint | 2608 m | 1391 m | 1474 m | 1474 m |
| Ground Resolution | 5,094 m | 1,358 m | 2,880 m | 1,440 m |

*Table 5: Four different sensing options for SC1 (CCD pixel size 10 x 10 microns)*

Using these figures, the following results had to be obtained with experiments and theoretical considerations:

1. DEM accuracy vs. sensing and algorithmic parameters (focal length, base angle, rotation between stereo partners, calibration problems) (Sections 9.3.2, 9.3)
2. DEM generation robustness for flat illumination conditions (rate of unmatchable areas) (Section 9.3.2)

## 3.2 SC2 DEM Generation from Lander Motion Stereo

### *3.2.1 SC2 Mission Profile Description*

This strategy component performs Lander segment landing site selection (LSLS) which enables the lander to autonomously select a safe touch down spot at a very late moment during descent. It requires a short hovering phase at a ground distance of about 200 meters. Hovering distance (horizontally) is about 70 meters forth and 35 meters back during the rest of the descent (Figure 2). Additional waiting of some 10 seconds is required for on-board processing of a DEM and slope hazard detection. In this scenario, the surrounding of the landing spot can be mapped with high resolution sufficient for a microrover application.

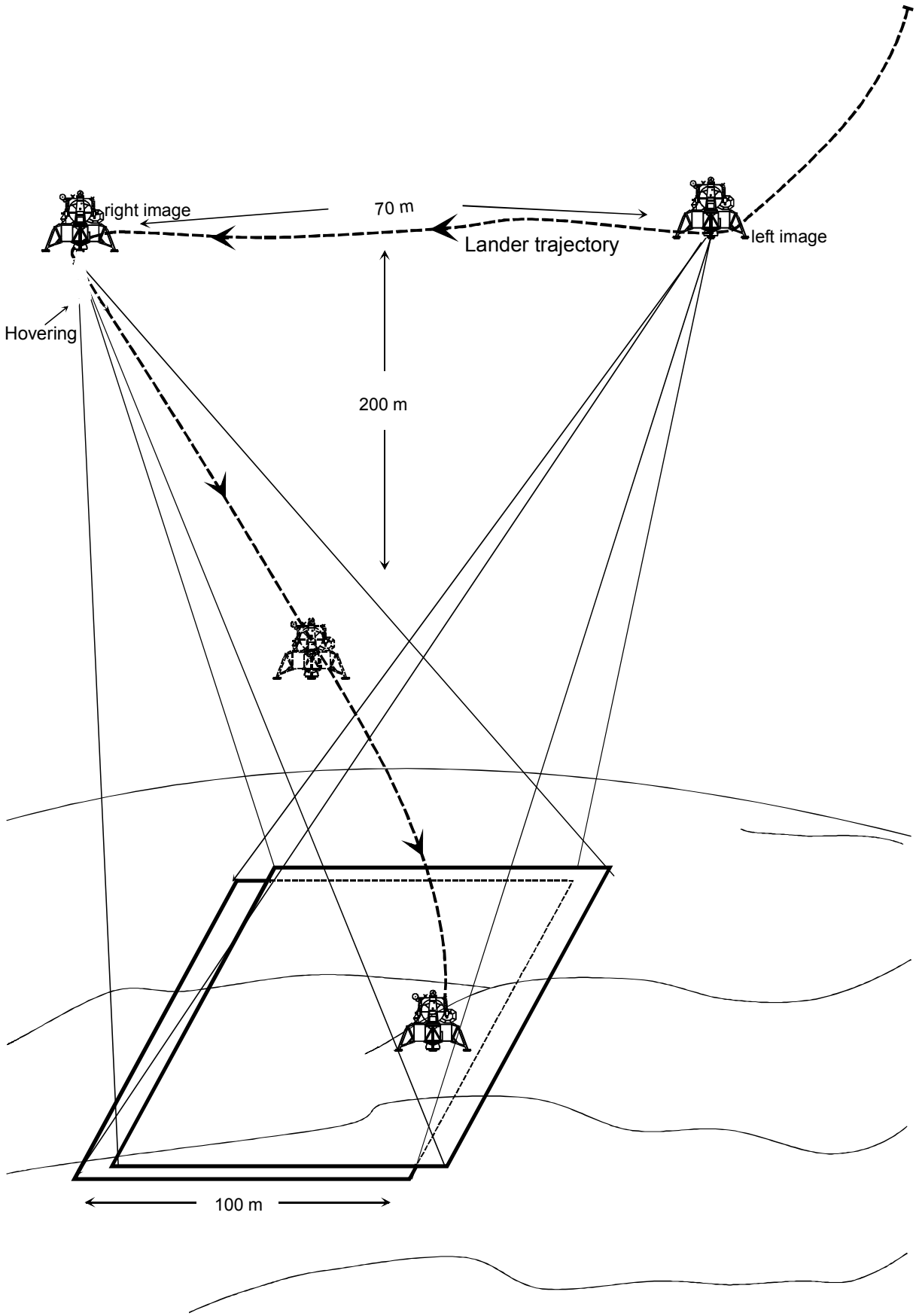


*Figure 2: Geometric scenario of SC2*

### 3.2.2 SC2 Requirements and Limitations (mission/environment)

1. To keep the landing site in the FOV, the lander must navigate and place the camera sufficiently accurate (see Table 6).
2. The hovering phase necessary for processing may cause errors in inertial navigation. This implies the necessity of vision based navigation to get the lander position with respect to the reconstructed area when the descent is continued. A simplified version of the procedure used for position initialization can be applied therefor (Section 4.2).
3. Since the processing of the DEM requires a high amount of computation power, it can only be performed once. A high level decision process has to be placed in front to select a proper candidate area. This could be driven by histogram analysis (large shadow areas should be avoided), low resolution disparity analysis or the usage of low resolution laser mappers as well as narrow-beam radar altimeters to estimate the overall slope of the scene currently viewed.
4. It must be guaranteed that the lander can reach any location within the mapped area after the safest spot has been identified.

### 3.2.3 SC2 Sensing/Processing Components

The procedure of landing site selection from the lander consists of three components:

1. Get (calibrate) the lander position. This can be done either by tracking from the initial descent height (Section 4.3, if an orbit DEM is available) or performing self-calibration (Section 9.5). Since the image resolution in this application is much higher than the resolution of the orbit, the self-calibration alternative is preferred. In that case one absolute distance measurement is required. The resulting (absolute) accuracy of the 3D reconstruction is not better than this measurement. This means, for 1 % accuracy of a LRF or radar altimeter, the DEM accuracy is at least worse than 1 %. However, since the self-calibration process provides a consistent calibration up to a scale factor, the DEM is still usable to get hazardous areas. It can be refined later on Earth if reference points are known after landing.
2. Calculate the DEM and ortho image from the stereo images and the calibrations.
3. Select a safe landing site by slope analysis.

The demands on sensing components are not very constraining, whereas the processing HW performance must be very high. The following tools must be available:

- One CCD array WAC with footprint in the range of the landing site width (Table 6).
- 1-2 MB storage, in case of LSLS 16 MB.
- Distance sensor to measure at least one distance to ground (if self-calibration option is chosen, see above).
- Reconstruction & calibration Hardware

### 3.2.4 SC2 Relevance, drawbacks and benefits

Even if a high resolution elevation model is not used for landing, the image acquisition geometry using a horizontal motion component during the late landing phase is a valuable prerequisite for reconstruction of the landing site on Earth for a microrover mission.
One major advantage of the LSLS approach is that in this case the lander is not dependent on a precalculated DEM from orbit. Furthermore the accuracy of the lander DEM is in any case sufficient for a safe landing. No landmark tracking is

necessary, the inertial sensor accuracy may be good enough to drive the lander to the automatically proposed landing site without further vision support.

### *3.2.5 SC2 Relevant Parameters and Experiments*

Table 6 shows three different options for an optical instrument on the lander. The third option is also given in Table 5, Entry (A). The figures may be scaled linearly to an image acquisition distance less than 200 meters leading to better resolution but smaller footprint. The required pointing accuracy of the first two options fit well into the given values. For Option LC, the pointing of the camera has to be performed using quick camera positioning engines, since the SC attitude control might be too coarse to provide proper pointing angles.

| | LA | LB | LC |
|---|---|---|---|
| N. of CCD Pixels | 512 x 512 | 1024 x 1024 | 512 x 512 |
| Focal Length | 10 mm | 20 mm | 40 mm |
| FOV | 28 deg | 28 deg | 14 deg |
| Ground Resolution (200 m Distance) | 0.2 m | 0.1 m | 0.05 m |
| Footprint (200 m Distance) | 100 m | 100 m | 25 m |
| Required Pointing Accuracy (90 % Overlap) | 1.4 deg | 1.4 deg | 0.35 deg |
| Required Inertial Sensing Accuracy | 10 m | 10 m | 2.5 m |

*Table 6: Three different sensing options for lander imagery (CCD pixel size 10 x 10 microns)*

Experimental results concerning accuracy can be derived from the SC1 experiments. Additional experiments and theoretical considerations were performed in terms of self-calibration and its effect on DEM generation:

1. Influence of disparity errors on self-calibration accuracy (Section 9.5)
2. Errors vs. base height ratio (Section 9.3.1)

## 3.3 SC3 Landing Site Mapping from Lander Stereo Cameras

### *3.3.1 SC3 Mission Profile Description*

Two cameras mounted on the lander with a reasonable base distance (more than one meter, Figure 3) can serve as stereoscopy system that provides images for terrain mapping at the last few hundred meters of descent. Any trajectory is possible during this phase, as long as the cameras are pointing towards the area to be mapped.

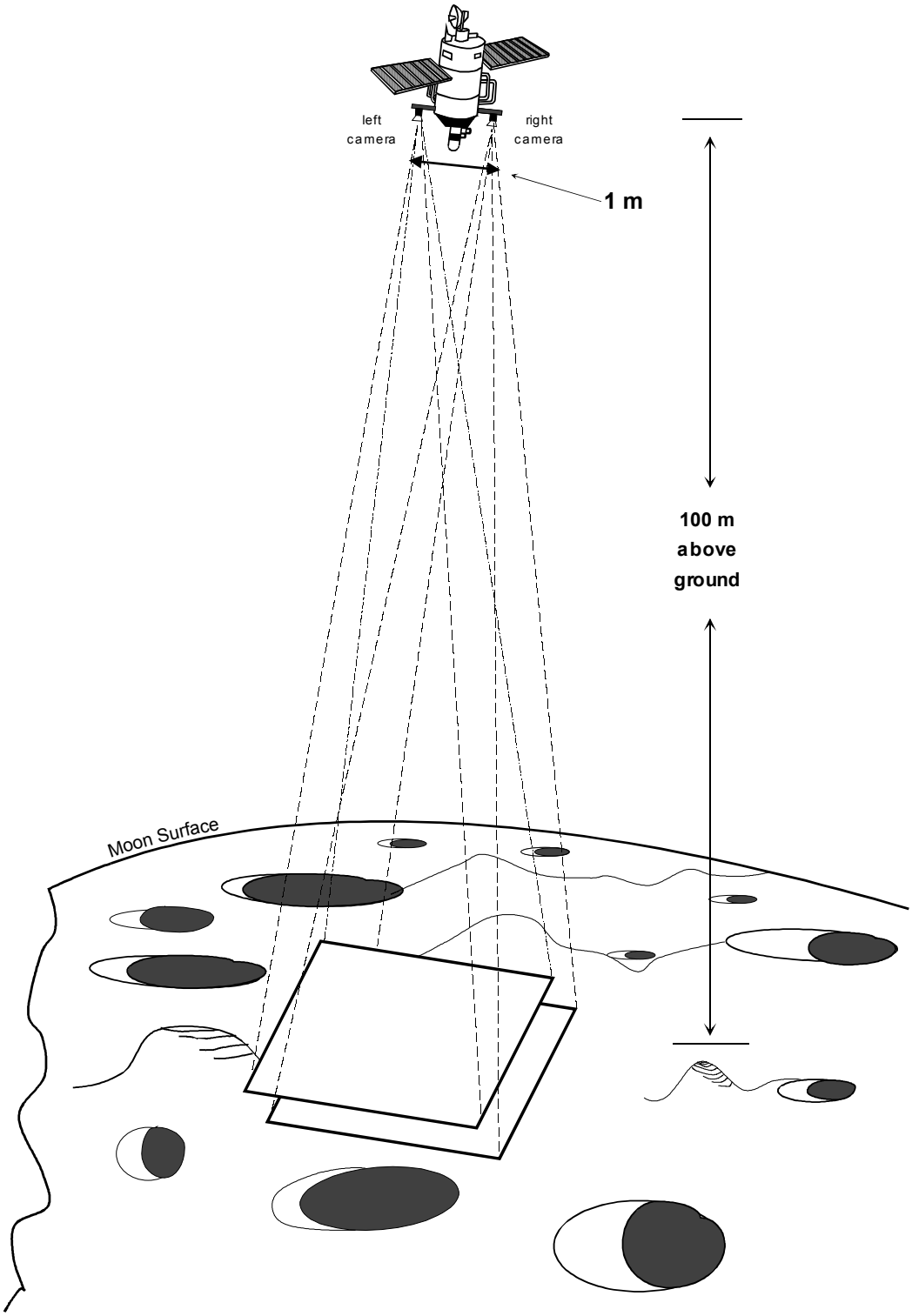


*Figure 3: Geometric scenario of SC3: Stereo cameras on the lander*

### *3.3.2 SC3 Requirements and Limitations*

1. To keep the landing site in the FOV, the lander must place the cameras sufficiently accurate (See Table 6).
2. The applicability of stereoscopy in such a configuration is restricted by the relatively small base (distance between stereo cameras). Therefore, only the last few hundred meters ground distance are of interest.

3. During landing, vibrations caused by thruster actions might cause miscalibrations and hence inaccuracy of the terrain reconstruction.
4. Utilizing the system for hazard detection implies strong requirements to the computational performance.

### 3.3.3 SC3 Sensing/Processing Components

- Two CCD array WACs mounted more than 1m apart from each other on the SC
- Processing Hardware

### 3.3.4 SC3 Relevance, Drawbacks and Benefits

The first advantage of stereo cameras on the lander to stereo from lander motion (Section 3.2) is that no additional maneuvers of the lander are necessary. The second advantage is the missing requirement of self-calibration: The stereo camera setup can be calibrated on Earth, and possibly checked in-flight using artificial landmarks on the lander itself.

The biggest disadvantage is the poor resolution of the system caused by the small base/height ratio. However, at near distances (<30 m) the system is able to acquire images for high resolution stereo mapping which could be used for the early stages of rover path planning.

### 3.3.5 SC3 Relevant Parameters and Experiments

1. Evaluate accuracy of DEM generation (Section 9.3.2)

# 4 NAVIGATION

## 4.1 SC4 Tracking of Crater Rim

### *4.1.1 SC4 Mission Profile Description*

In case of the particularly proposed mission scenario that foresees landing at the rim of a crater, near the shadow border, this border can be tracked easily and efficiently using low complexity image processing methods. This strategy may be chosen if the target crater is large in comparison with the Ellipsis of Uncertainty.

If the crater rim is oriented orthogonal to the entry direction and the across-track error is small, tracking of the shadow border together with distance measurements by additional sensors can lead to very accurate touch-down directly at the shadow border.

### *4.1.2 SC4 Requirements and Limitations (mission/environment)*

To easily identify the correct crater rim at the beginning of the descent, its features must be known exactly. Simplest approach is applicable if the crater is the biggest one in any of the expected field of views: The largest dark area is the shadow caused by the crater rim.
The touch-down accuracy depends on the width of the transition area between illuminated side and shadow side of the rim. If the ridge is very sharp, it can be located better.

### *4.1.3 SC4 Sensing/Processing Components*

- One CCD array WAC
- Segmentation hardware

### *4.1.4 SC4 Relevance, drawbacks and benefits*

Although the application of crater tracking depends heavily on the environment and terrain conditions, its feasibility is high once these conditions are given.
The processing complexity of the algorithm is very low, hence the update rate. The method does not depend on calibration
If the landing site is not fixed on a specific crater, the decision can be made during beginning of descent. Finding craters in flatly illuminated regions is a relatively simple segmentation problem. If the illumination direction is known, the rim should be identified unambiguously. Since no a priori information about calibration parameters or terrain morphology is necessary, the criterion to find a crater rim may result in a very robust hazard avoidance strategy.

### *4.1.5 SC4 Relevant Parameters and Experiments*

No software is currently available that does the specific tasks described above. Nevertheless the following can be done:

1. Illuminate the MOON mockup using different angles and look at the morphological appearance of crater rims (Section 9.6)

## 4.2 SC5 Position Initialization from Reference Images

### *4.2.1 SC5 Mission Profile Description*

At the beginning of the descent, if the lander is at a height of 3-5 km above ground, the camera is looking at a region somewhere within the uncertainty region (EU, Figure 4).

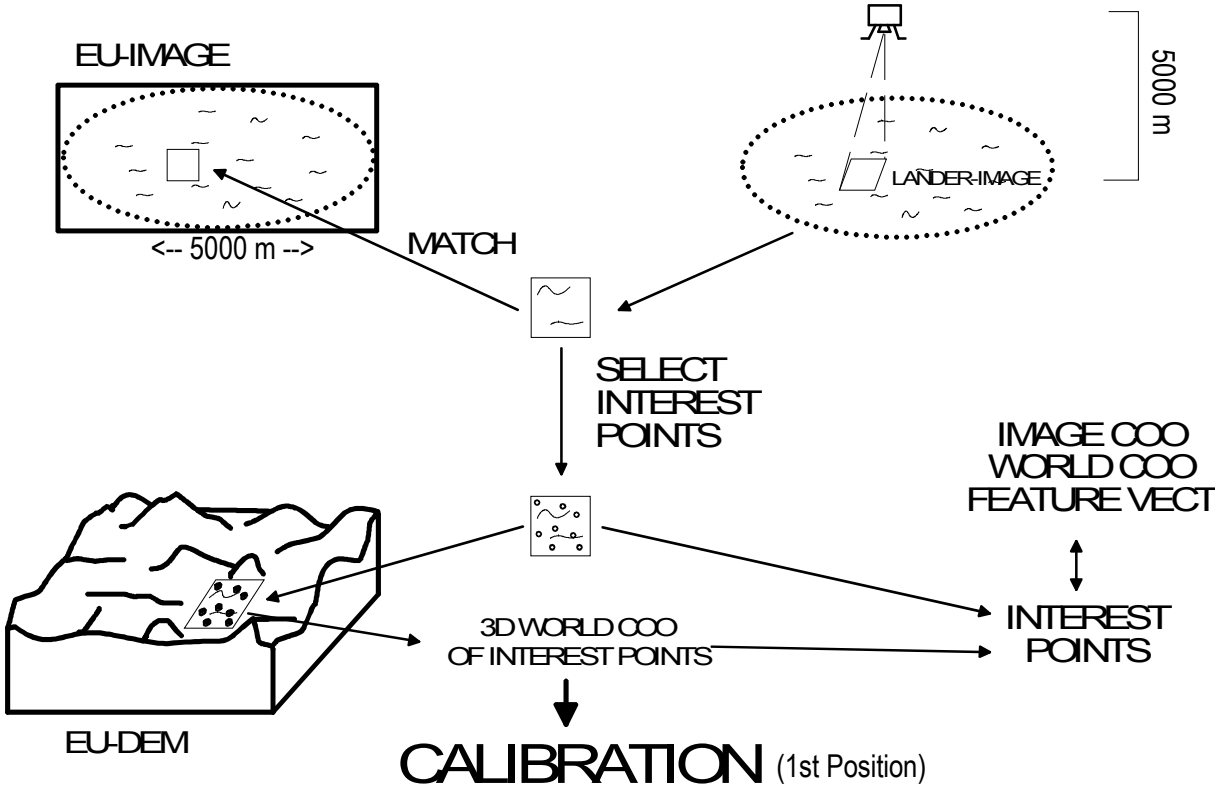


*Figure 4: Geometric & algorithmic scenario of SC5*

If a terrain model and ortho image of this region are available, the position of the lander can be calculated by image matching and calibration. Only one image is necessary, acquired from the lander in near vertical direction. This can be done at any stage of descent, as long as the resolution of the ortho image, with respect to the lander image, is sufficient.

### *4.2.2 SC5 Requirements and Limitations (mission/environment)*

1. DEM and ortho image should have been generated with the same illumination conditions as given during descent.
2. The rotation between ortho image and the acquired view should not exceed 10°.
3. Viewing angle should not differ more than 30° from the local vertical.

### *4.2.3 SC5 Sensing/Processing Components*

Sensing components are the same as for SC2 (Section 3.2). Processing must perform matching between ortho image and lander image, and calibration.

### *4.2.4 SC5 Relevance, drawbacks and benefits*

If a preselected landing site should be reached with high accuracy (10 - 100 meters), the navigation based on landmarks is one of the major candidates that are currently available. Its first component is a good estimation of the lander position at beginning of descent.

Processing of the first lander image and comparison with the EU image could be performed on ground, since the reaction time can be more than half a minute (considering 5 km distance and 10 m/sec descent speed). In this case the next image for landmark tracking (see Section 4.3) can be acquired after reception of the initial position (at an altitude of about 4.5 km).

### *4.2.5 SC5 Relevant Parameters and Experiments*

Candidates for sensors have already been described in Section 3.1.5, Table 5. Following experiments were necessary to verify the functionality of the proposed algorithms:

1. Position and pointing accuracy dependent on disparity errors (Section 9.4)
2. Accuracy vs. viewing angle (Section 9.7.1)
3. Accuracy vs. DEM resolution (Section 9.7.1)
4. Testing several real situations (Section 9.7)

## 4.3 SC6 Landmark Tracking for Position Update

### *4.3.1 SC6 Mission Profile Description*

Once a position of the lander is known with good accuracy (Section 4.2), the update of the position with required rate (about 0.1 Hz) can be accomplished by landmark tracking (Figure 5). The trajectory profile during descent can be of any form, as long the camera pointing is known with sufficient accuracy (see below).

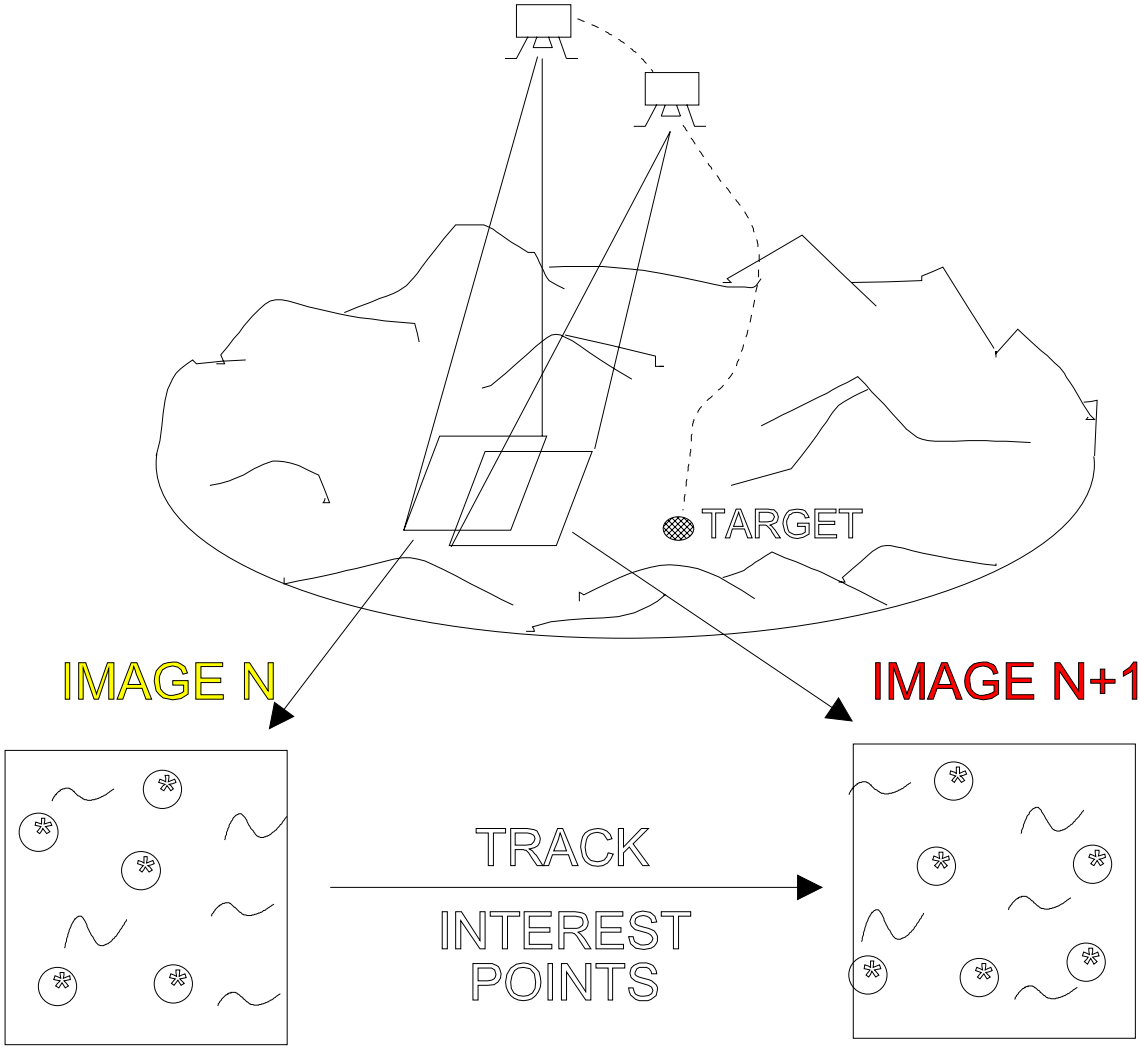


*Figure 5: Algorithmic scenario of SC6*

### *4.3.2 SC6 Requirements and Limitations (mission/environment)*

1. A DEM must be available in sufficient accuracy.
2. In case of a guided descent and a high amount of horizontal motion, the tracking rate (images/time) must be increased according with the horizontal distance to the target area to realize a sufficient overlap between two subsequent images. If this is not possible, the camera has to be tilted. In this case, vision based navigation will terminate if the view gets too flat. One solution to this problem would be to initialize the position one more time using a view towards the landing site and keeping the

landing site within the field of view. However, a scenario with such a high horizontal motion component is not realistic.

### 4.3.3 SC6 Sensing/Processing Components

Sensing components are the same as for SC2 (Section 3.2). Processing must perform landmark tracking and calibration.

### 4.3.4 SC6 Relevance, drawbacks and benefits

- If a DEM is available from orbit, the landmark based tracking, as a continuation of the position initialization, can be a valuable tool to support the navigation system.
- It can refine the distance measurements, since accuracy in z is about 0.1 % of range in practical experiments.
- Due to its relatively long update rate, the landmark tracking is robust over a long period and can serve as backup or concurrence system to the (integrating) horizontal motion measuring systems.
- In its sophisticated version, 3D landmark tracking can be used in a closed-loop landing to reach a predefined landing spot accurately.
- The necessary update rate still allows transmission of the images to Earth and processing on ground.
- At the first quarter of the descent the scale between two subsequent images does not change very much. Therefore, a set of some images can be used for tracking. The results can be filtered to enhance calibration accuracy.

### 4.3.5 SC6 Relevant Parameters and Experiments

Having an update rate of 0.1 Hz (10 seconds per image), every 100 meters an image has to be taken. The current algorithm allows a scale change of at least 20 % which means that, with this update rate, the system works until 500 meters ground distance. Higher update rates can be accomplished by a reduction of the image resolution and/or number of landmarks used for calibration.
Following experiments were performed:

1. Accuracy vs. number of tracking positions (Figure 16)
2. Accuracy vs. number of landmarks (Figure 18)
3. Robustness against errors in first position (Figure 14, Figure 15)
4. Testing several real situations (Section 9.8)
5. Accuracy vs. image resolution (interesting for last stages of descent) (Figure 17)

# 5 MOTION MEASUREMENT BY VISION

## 5.1 SC7 2D Lateral Motion Evaluation

### *5.1.1 SC7 Mission Profile Description*

A simplified version of 3D landmark tracking can be performed in 2D as well. For that reason, the same geometry as depicted in Figure 5 can be used. Any trajectory profile is possible, the camera should point near vertically down.

### *5.1.2 SC7 Requirements and Limitations (mission/environment)*

1. One narrow angle distance measurement coupled to the camera is necessary. Coordinates of its footprint should be known within the image. If the distance measurement FOV covers more than one pixel, its properties in terms of integration within this FOV („Weight per pixel“) must be known.
2. Overlap between the images should be kept as high as possible. However, during large horizontal motions there is a tradeoff between overlap and maintenance of the viewing direction.

### *5.1.3 SC7 Sensing/Processing Components*

Sensing components are the same as for SC2 (Section 3.1.3). Processing must perform tracking and self-calibration.

### *5.1.4 SC7 Relevance, drawbacks and benefits*

Even if a distance measurement is not available, the horizontal velocity can be determined relatively up to a scale factor.

### *5.1.5 SC7 Relevant Parameters and Experiments*

Mockup: Compare measured distance to CamRobII (Section 9.1) displacement (Section 9.9)

# 6 HAZARD DETECTION

## 6.1 SC8 Hazard Avoidance from 2D Lander Image

### *6.1.1 SC8 Mission Profile Description*

This strategy component detects obstacles and hazardous slopes from radiometric image response. Especially in flatly illuminated regions, obstacles can easily be found using their shadows. Using a WAC as proposed in the SOW, at a distance of 500 m obstacles with 2.5 m diameter can be detected (smaller obstacles if illumination very flat). The required size of 0.5 m is detected at a distance of 100 m which gives about 5 seconds reaction time since processing can be performed within approx. 1 second. If the distance from ground is known from additional sensors (radar altimeter), the size of the obstacles found can be estimated with accuracy in the range of the distance measurement accuracy.

### *6.1.2 SC8 Requirements and Limitations (mission/environment)*

To keep the landing site in the FOV, the lander must navigate and place the camera sufficiently accurate (see Table 6). If the illumination angle is flat, relatively small objects cause large shadow areas thereby leading to misclassification of safe areas.
One problem is that some prior knowledge about the object distribution and size in the area of interest must be given to select proper parameters for the currently available algorithm.

### *6.1.3 SC8 Sensing/Processing Components*

- One CCD array WAC
- Distance sensor to measure at least one distance to ground to estimate the obstacle (shadow) size.
- Segmentation hardware

### *6.1.4 SC8 Relevance, drawbacks and benefits*

Hazard detection from object shadows and grey level segmentation is a very quick process that can be used as backup decision and to support other sensors. The current update rate of 1-2 seconds is very promising for application shortly before touch-down. No calibration is necessary, the system can work stand-alone even if only very rough estimates of ground distance (+/-50 %) are available.

### *6.1.5 SC8 Relevant Parameters and Experiments*

As baseline WAC the figures given in Table 6 are used.
The required pointing accuracy is in the order of those given there.

Following analysis had to be obtained:

1. Reconnaissance of objects: Size vs. illumination angle (Section 9.10)

## 6.2 Hazard Avoidance from 3D Lander Terrain Mapping

The process of lander stereo terrain mapping is described in Sections 3.2 and 3.3. An additional slope analysis detects hazardous slopes from the DEM images.

# 7 RECOMMENDED STRATEGIES

This section describes two strategies that are different in complexity, performance and requirements. The first one is a „minimum strategy“ using computer vision only for 2D hazard detection before touch-down. The second is a complex closed-loop strategy that provides navigational information to the lander to enable a touch-down at a landing spot predefined on Earth. The strategy components described in the previous sections are combined, relevant parameters of the specific mission described in Section 2.3 are used to interface the components to get a realistic processing chain.

## 7.1 Hazard Detection for Safe Touch-Down

Detecting possible obstacles that can cause damage to the lander during touch-down is an important task to increase the probability of the mission success. In Section 6 the respective functional component is described. Obstacle detection begins at a ground distance of 200 m having an obstacle detection ability of better than 0.5 m obstacle diameter. Every second an image is taken, 1 second later the location of the best landing spot with respect to the FOV of the camera can be transmitted to the SC motion control. Since the process does not depend on other vision-based results, it can run independently to support the landing decision.

Optionally, the 2D hazard detection can also be used to detect slopes from grey-level images from higher distances. This is only useful if landing directly on a crater rim is not foreseen, since this would be a spot very close to a „probably hazardous area“.

## 7.2 Closed-Loop Predefined Spot Touch - Down

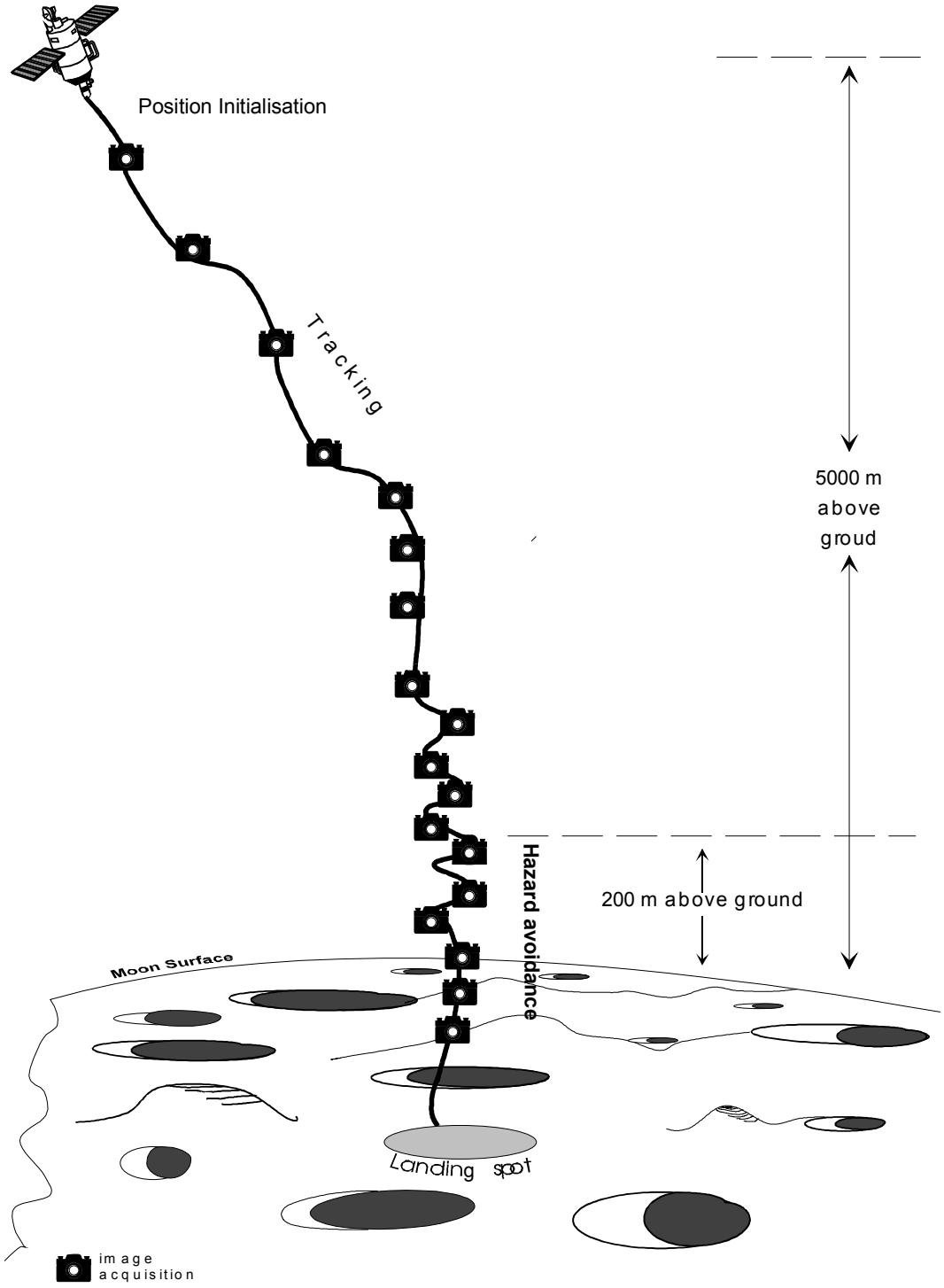


*Figure 6: Closed-Loop lander navigation for predefined spot touch-down*

This strategy utilizes all of the complex reconstruction and navigation algorithms introduced in the previous sections. Beginning with a 3D stereo reconstruction of the EU region from orbit, imagery of the whole EU region is sent to Earth to be processed there. Results of Earth processing are a high resolution DEM of the EU as well as an ortho image and the localization of one or more landing spots. These results are sent to the lander shortly before the beginning of the descent. At a ground distance of about 5 km, the lander initializes its position and predicts the maneuvers necessary to

reach the (nearest) predefined landing spot. Subsequent tracking and update of position as well as recalculation of the necessary reactions guide the lander to a position 200 m above the preselected landing spot. The final touch-down spot is obtained by 2D - obstacle detection, looking for the best candidate location (touch-down area without obstacles or slopes).

Figure 6 shows the whole chain to reach this goal, the actions are described in Table 7 The time figures of this scenario were provided by Jean de Lafontaine (ESA/ESTEC), without considering a possible hovering for horizontal positioning. Descent speed was assumed 20 m/sec above 1000 m ground distance and 10 m/sec below. In case of hovering, the update rate of about 5 seconds during landmark tracking can be continued during this phase.

| Time (seconds) | At ground distance | Action |
|---|---|---|
| -7000 | Orbit (15-25 km) | Acquire orbiter stereo images |
| -6990 - -4000 | Orbit | Send stereo images to Earth |
| -6990 - -3000 | *on Earth* | Process stereo images |
| -3000 - -500 | *on Earth* | Select landing site(s) |
| -5000 - -500 | *on Earth* | Transmit DEM and ortho image and landing site location(s) to lander |
| 0 | 5000 m | Start position initialization |
| 20 | 4760 m | Position initialized, necessary horizontal motion identified |
| 40 | 4500 m | Begin of navigation: First tracking image |
| 56, 76, 94, 112, 126, 139, 151, 160, 170, 178, 186, 194, 200, 206, 212, 222, 230, 238, 245, 252, 258, 253, 249, 254, 259, 264, 270 | 4100, 3690, 3320 ,2990, 2690, 2420, 2180, 1960, 1760, 1590, 1430, 1290, 1160, 1040, 940, 840, 760, 680, 620, 550, 490, 440, 400, 350, 300, 250, 200 m | • Subsequent tracking,<br>• position update after 5 seconds,<br>• feedback loop to motion reaction |
| 270,269,.....290 | 200,190,....30 m | 2D Obstacle detection, horizontal motion reaction after 1 second |
| 300 | 0 m | Touch - down |

*Table 7: Image acquisition times and actions for vision based navigation for Strategy 2: Closed loop Lander navigation*

# 8 HARDWARE

Underlying reference processing unit for all computing performance estimations is the STELLAR board [[Par94]] developed by British Aerospace. It comprises an ADSP21020 DSP processor and several memory components together with two separated bus structures (Figure 7). Table 8 shows the power consumption of the components. Estimated mass is **1 kg**, the components could be mounted on a single extended Eurocard or double Eurocard. Running at 20 MHz, the ADSP21020 DSP processor is capable of 20 MIPS when operating with zero wait-state memory, which results in a peak processing power of between 40 and 60 MFLOPS. Performance estimations were made considering a coding efficiency of 10 %.

An outline development schedule for the flight standard real-time processor is illustrated in Table 9.

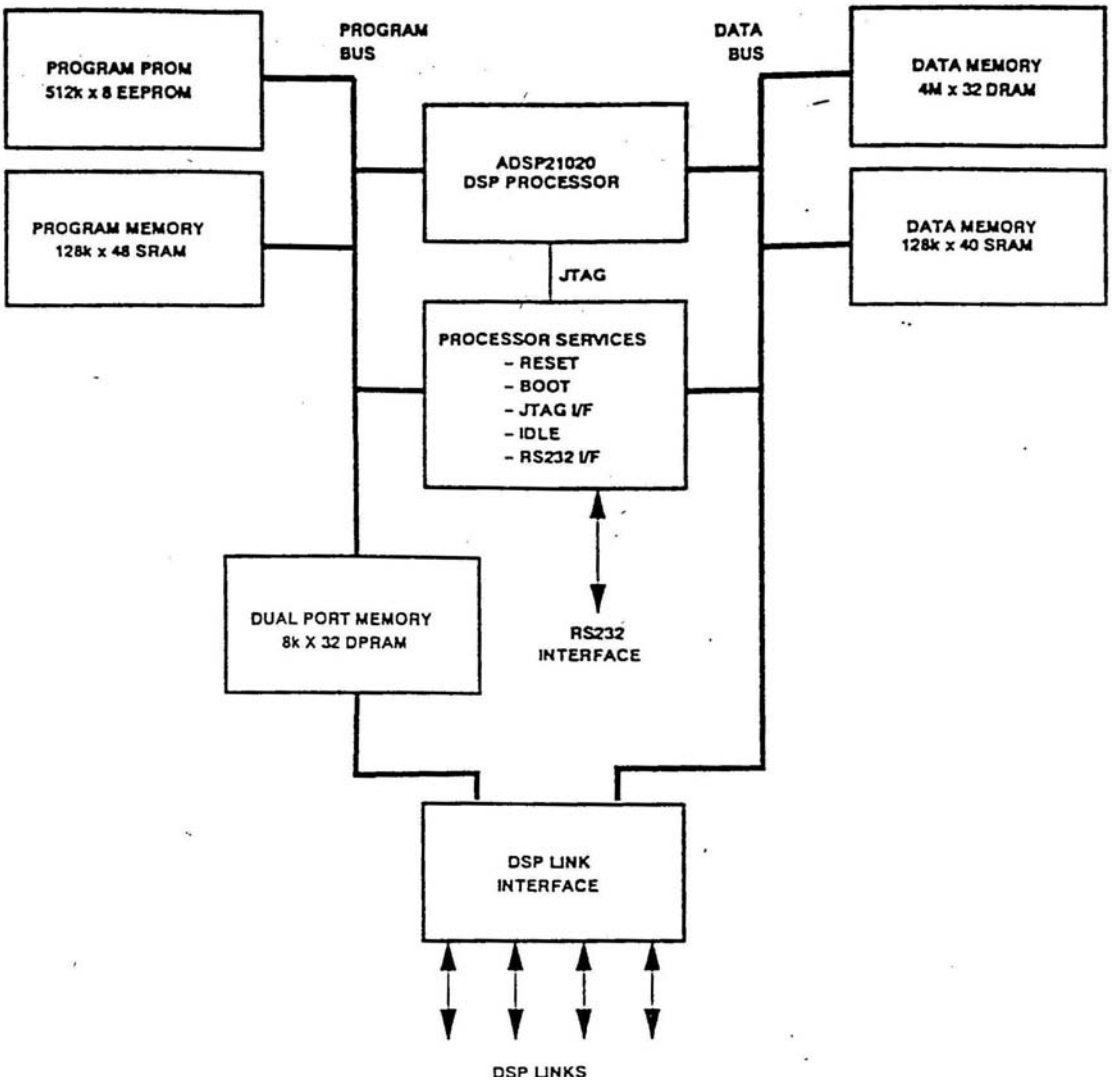


*Figure 7: Block Diagram of Flight Standard Real-Time Processor (STELLAR Board)*

| Item | Power per device (Watts) | No. of devices | Total Power (Watts) |
|---|---|---|---|
| DSP Processor | 2.4 W | 1 | 2.4 |
| Program SRAM 128k x 32 | 0.625 W | 6 | 3.8 |
| Dual Port Mem 8k x 32 | 2 W | 2 | 4.0 |
| Data SRAM 128k x 32 | 0.625 W | 5 | 3.1 |
| Data DRAM 128k x 32 | 0.4 W | 8 | 3.2 |
| Processor Services ASIC | 0.5 W | 1 | 0.5 |
| DSP-links ASIC | 2W | 1 | 2.0 |
| **TOTAL** | | **24** | **19.0** |

*Table 8: Flight Standard Real-Time Processor: Estimated Maximum Power Consumption*

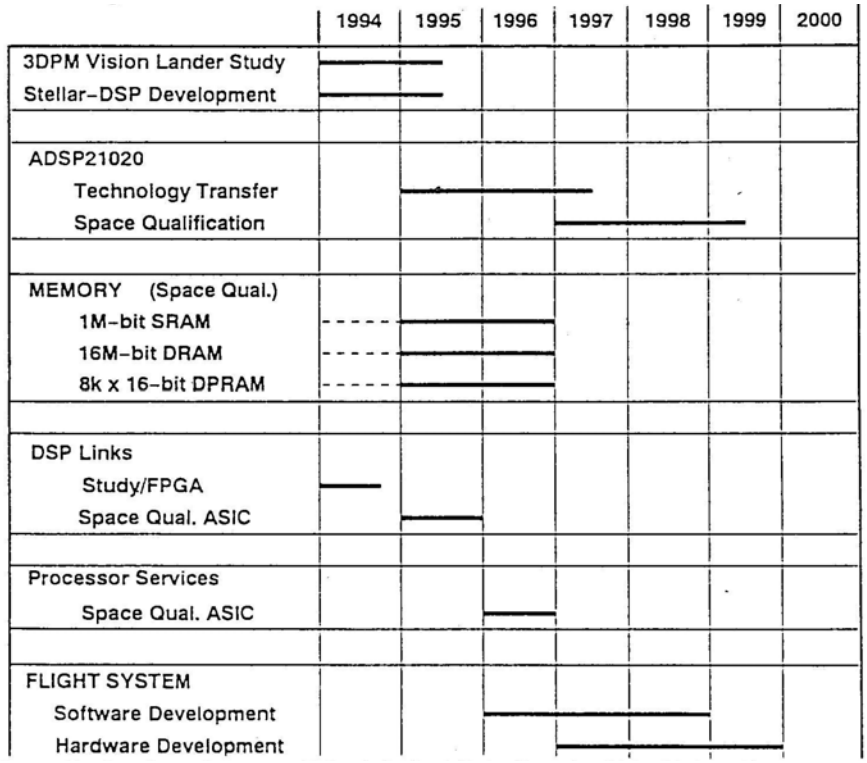


*Table 9: Outline Development Schedule for Flight Standard Real-Time Processor*

## 8.1 Computational Performance of the Algorithms

The analysis of the existing algorithms was taken from [[PSC+94]]. The underlying sensor is LA (Table 6, Page 15), except for SC1 where the orbiter camera D (Table 5, Page 12) is used. As hardware component, the STELLAR board is used as baseline.

| | | Memory Requirement | Comment |
|---|---|---|---|
| **SC1 DEM from orbit** | 1 hour (Sparc 20) + 1 hour (operator) | 64 Mbytes | Entire EU reconstruction on Earth |
| **SC2 DEM from lander motion** | 30 seconds | 16 Mbytes | Half resolution |
| **SC3 DEM from lander stereo** | 2 minutes (Sparc 20) | 16 Mbytes | No real-time requirement |
| **SC5 Position initialization** | 10 seconds | 10 Mbytes | |
| **SC6 Landmark tracking** | 3 seconds | 8 Mbytes | |
| **SC7 2D Lateral Motion** | 4 seconds | 8 Mbytes | |
| **SC8 2D Hazard detection** | 2 seconds | 4 Mbytes | Worst case |

# 9 ERROR BEHAVIOR OF EXISTING ALGORITHMS

## 9.1 Tools

To estimate errors of the vision system during a real mission, the following tools were used:

1. Mathematical analysis of the algorithms (See Appendix A)
2. Experiments using artificially rendered images. The underlying texture and DEM were taken from a real mockup scene.
3. Experiments using the high precision camera pointing device CamRobII by JOANNEUM RESEARCH [[PSC+94]]. This tool provides accurate reference coordinates for evaluation of navigation and reconstruction accuracy.
4. SW components developed during the PBMT1 study

In the laboratory experiments a scale factor of 1:3000 was assumed. 1 mm in this model corresponds to 3 m in reality.

## 9.2 Disparity Map Generation

The following steps were performed to investigate the error rate during disparity map generation:

1. Generate two artificial views from a real scene, using the corresponding DEM (which may contain some errors, this is not relevant for the procedure)
2. Calculate a reference disparity map using the viewing parameters of these views and the DEM
3. Calculate a disparity map from the views using the matching algorithm HFVM
4. Compare reference and disparity maps

Figure 8 shows the disparity errors (RMS) for a set of artificial stereo configurations. Knowing about the effects of different rotation angles between the stereo partners and different base/height ratios (expressed by the difference in viewing angle) on the disparity errors allows to find the reasonable limits in stereo image acquisition. Border effects were neglected as well as obvious mismatching errors that were detected during 3D reconstruction (see Section 9.3).

**Major result of this experiment is the expected RMS disparity error of 0.4 pixels for realistic configurations.**

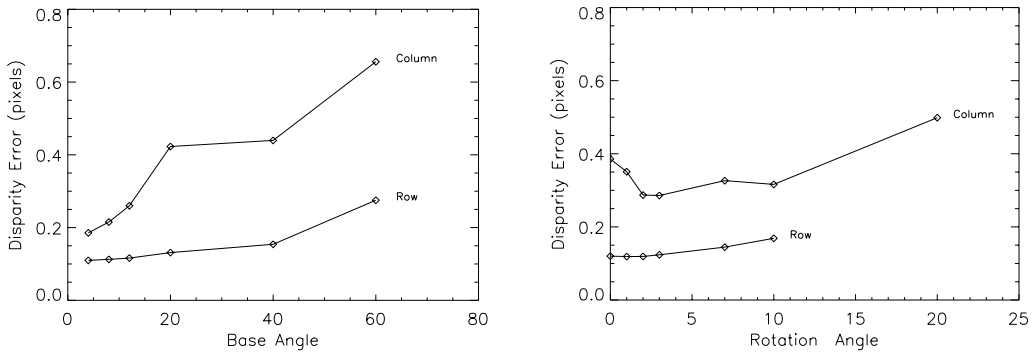


*Figure 8: Disparity errors dependent on imaging geometry. Base angle is the vergence angle (Image centers point towards the same surface point), the rotation angle was varied at a base*

*angle of 30 degrees. The images were rendered using the moon mockup DEM. Angles are given in Gons. 100 Gons = 90 degrees*

## 9.3 3D Reconstruction (Locus Method)

### *9.3.1 Theoretical Aspects*

Three different sources can cause errors during reconstruction:

- Errors in the disparity map
- Calibration errors
- Discretization errors in the Locus algorithm

The latter can be neglected due to [[Bau94]]. Table 10 shows the dependencies between different types of errors for a set of realistic camera models and stereo setups, taking into account both orbit and lander imagery.
**These results show that the expected disparity error of 0.4 pixels does not heavily contribute to DEM generation errors compared to calibration errors. The expected error is about 2 meters (elevation) using a typical sensor with 100 mm focal length (option C), 25 km ground distance and 30 degrees base angle.**

| A (f=40 mm, 512 x 512 pixels) dist.=15km | | | | | | | | |
|---|---|---|---|---|---|---|---|---|
| **deg** | **base/height** | **0.1** | **0.2** | **0.4** | **0.7** | **1.0** | **1.0** | **1.5** |
| 4 | 0,069842 | 5,369 | 10,739 | 21,477 | 37,585 | 53,693 | 61,999 | 92,999 |
| 8 | 0,139854 | 2,681 | 5,363 | 10,723 | 18,770 | 26,814 | 30,962 | 46,442 |
| 16 | 0,281082 | 1,334 | 2,668 | 5,337 | 9,339 | 13,341 | 15,405 | 23,108 |
| 30 | 0,535698 | 0,700 | 1,400 | **2,799** | 4,898 | 6,998 | 8,080 | 12,120 |
| 60 | 1,154701 | 0,325 | 0,650 | 1,299 | 2,273 | 3,248 | 3,750 | 5,625 |
| **B (f=150 mm, 1024 x 1024 pixels) dist.=15km** | | | | | | | | |
| **deg** | **base/height** | **0,1** | **0,2** | **0,4** | **0,7** | **1,0** | **1,0** | **1,5** |
| 4 | 0,069842 | 1,432 | 2,864 | 5,727 | 10,023 | 14,318 | 16,533 | 24,800 |
| 8 | 0,139854 | 0,715 | 1,430 | 2,860 | 5,005 | 7,150 | 8,256 | 12,385 |
| 16 | 0,281082 | 0,356 | 0,712 | 1,423 | 2,490 | 3,558 | 4,108 | 6,162 |
| 30 | 0,535698 | 0,187 | 0,373 | **0,746** | 1,306 | 1,866 | 2,155 | 3,232 |
| 60 | 1,154701 | 0,087 | 0,173 | 0,346 | 0,606 | 0,866 | 1,000 | 1,500 |
| **C (f=100 mm, 512 x 512 pixels) dist.=25km** | | | | | | | | |
| **deg** | **base/height** | **0,1** | **0,2** | **0,4** | **0,7** | **1,0** | **1,0** | **1,5** |
| 4 | 0,069842 | 3,580 | 7,159 | 14,318 | 25,057 | 35,795 | 41,333 | 61,999 |
| 8 | 0,139854 | 1,788 | 3,575 | 7,150 | 12,513 | 17,876 | 20,641 | 30,962 |
| 16 | 0,281082 | 0,889 | 1,779 | 3,558 | 6,226 | 8,894 | 10,270 | 15,405 |
| 30 | 0,535698 | 0,467 | 0,933 | **1,866** | 3,266 | 4,665 | 5,387 | 8,080 |
| 60 | 1,154701 | 0,217 | 0,433 | 0,866 | 1,516 | 2,165 | 2,500 | 3,750 |
| **D (f=200 mm, 512 x 512 pixels) dist=25km** | | | | | | | | |
| **deg** | **base/height** | **0,1** | **0,2** | **0,4** | **0,7** | **1,0** | **1,0** | **1,5** |
| 4 | 0,069842 | 1,790 | 3,580 | 7,159 | 12,528 | 17,898 | 20,666 | 31,000 |
| 8 | 0,139854 | 0,894 | 1,788 | 3,575 | 6,257 | 8,938 | 10,321 | 15,481 |
| 16 | 0,281082 | 0,445 | 0,889 | 1,779 | 3,113 | 4,447 | 5,135 | 7,703 |
| 30 | 0,535698 | 0,233 | 0,467 | **0,933** | 1,632 | 2,333 | 2,693 | 4,040 |
| **60** | 1,154701 | 0,108 | 0,217 | 0,433 | 0,758 | 1,083 | 1,250 | 1,875 |

*Table 10: Expected Locus reconstruction errors (meters) depending on disparity errors*

### *9.3.2 Experiments*

To estimate the influence of illumination to DEM generation accuracy, experiments with 3 different illumination angles were performed:

The same stereo configuration was used for all three experiments. The reference DEM had been acquired using stereo from closer positions and merging a set of e reconstruction results (Figure 11). Table 11 lists the results. Having a scale factor of 3000, the imaging sensor would correspond to reference sensor A (4m ground resolution).

| | max error | RMS error (*z*) | % valid elevations |
|---|---|---|---|
| **8° illumination** | 54.57mm | 2.60mm | 27 |
| **10° illumination** | 23.94mm | 2.24mm | 33 |
| **20° illumination** | 78.92mm | 2.44mm | 61 |

*Table 11: DEM generation errors depending on illumination angle (scale 1:3000)*

The total number of DEM pixels on the reference DEM was 851851. The left stereo component and the difference DEM for the 8° illumination case are depicted on Figure 9. No significant influence of illumination angle on the RMS error could be detected. **The extrapolation of this mockup experiment to reality using a scale factor of 3000 results in DEM RMS errors in the range of 6 - 7 meters**. Maximum errors occurred at the borders of the FOV, hence are not significant for the inner part of the DEM.
One source of the RMS error is the reference DEM, since it was merged from many stereo configurations. At the borders between these components, some inaccuracies in the range of 1-2 mm were detected. They are the main contributions to the relatively large errors displayed above.

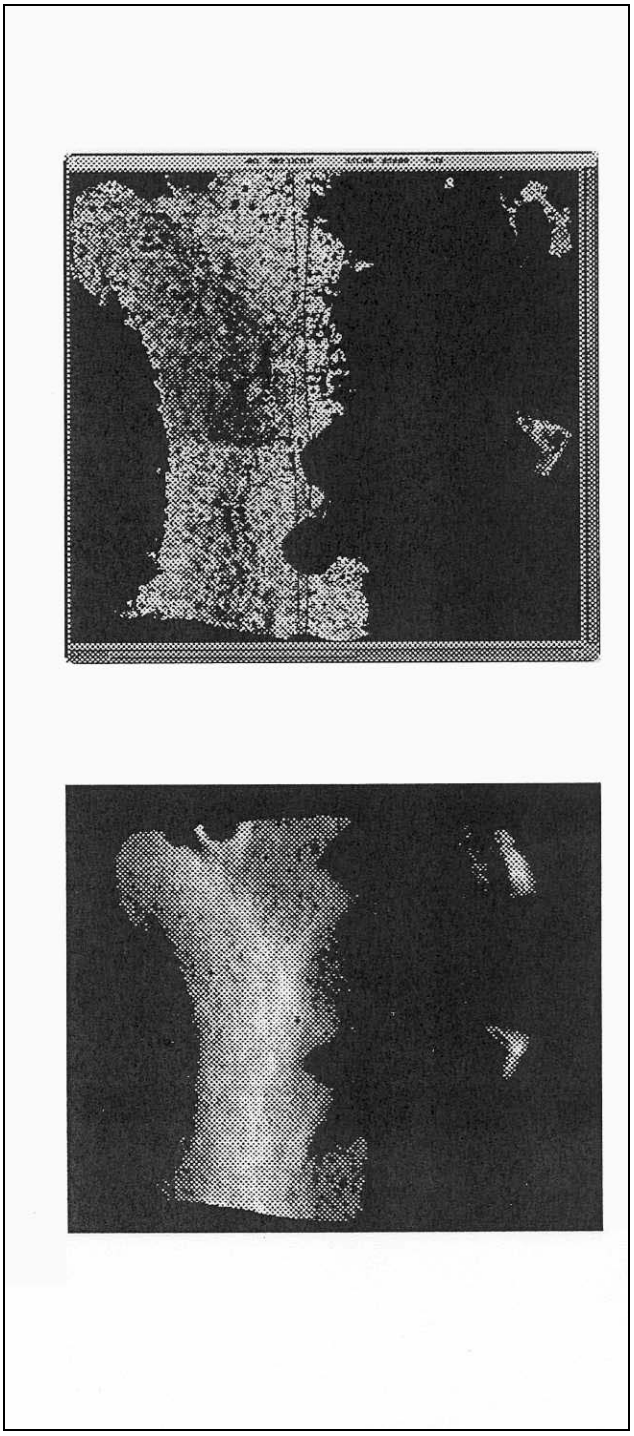

*Figure 9: Ortho image (below) and DEM reconstruction difference to reference for 8 degrees illumination. Range of difference is between -3mm (black) and +3mm (white).*

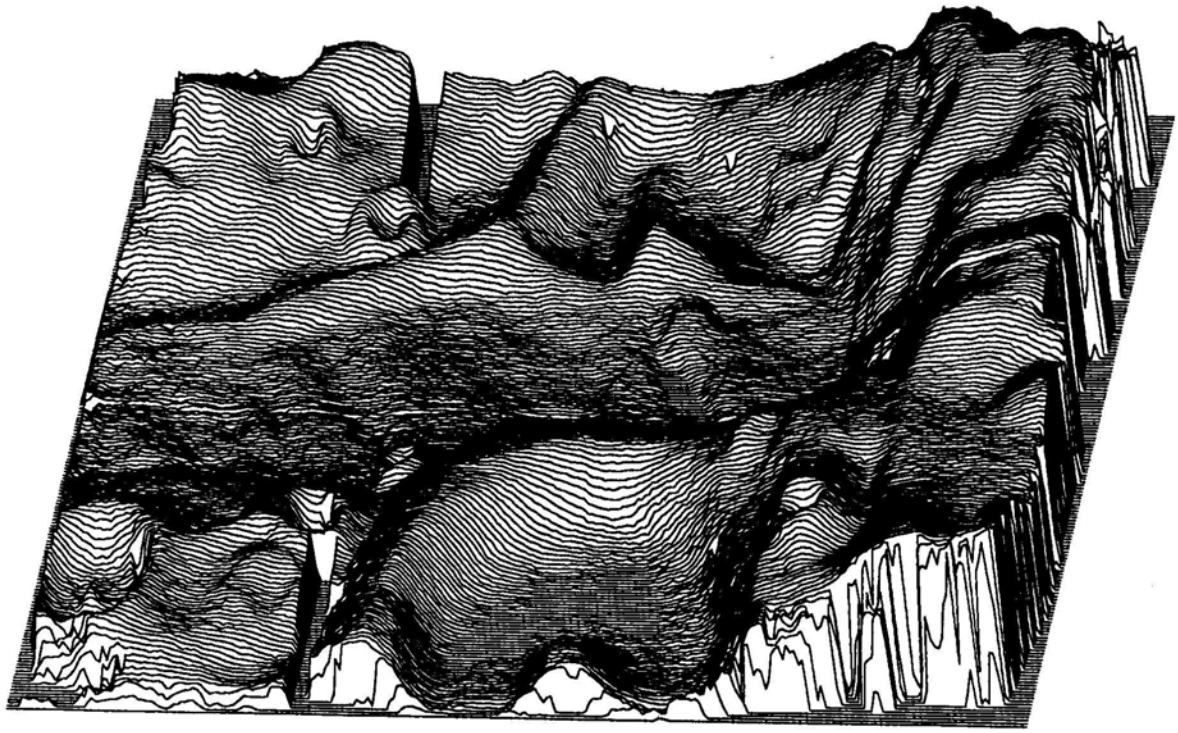

*Figure 10: DEM of laboratory moon mockup. Size is 1500 x 2000 mm, elevation range 50-250mm, pixel resolution 1 mm (slightly misscaled in x)*

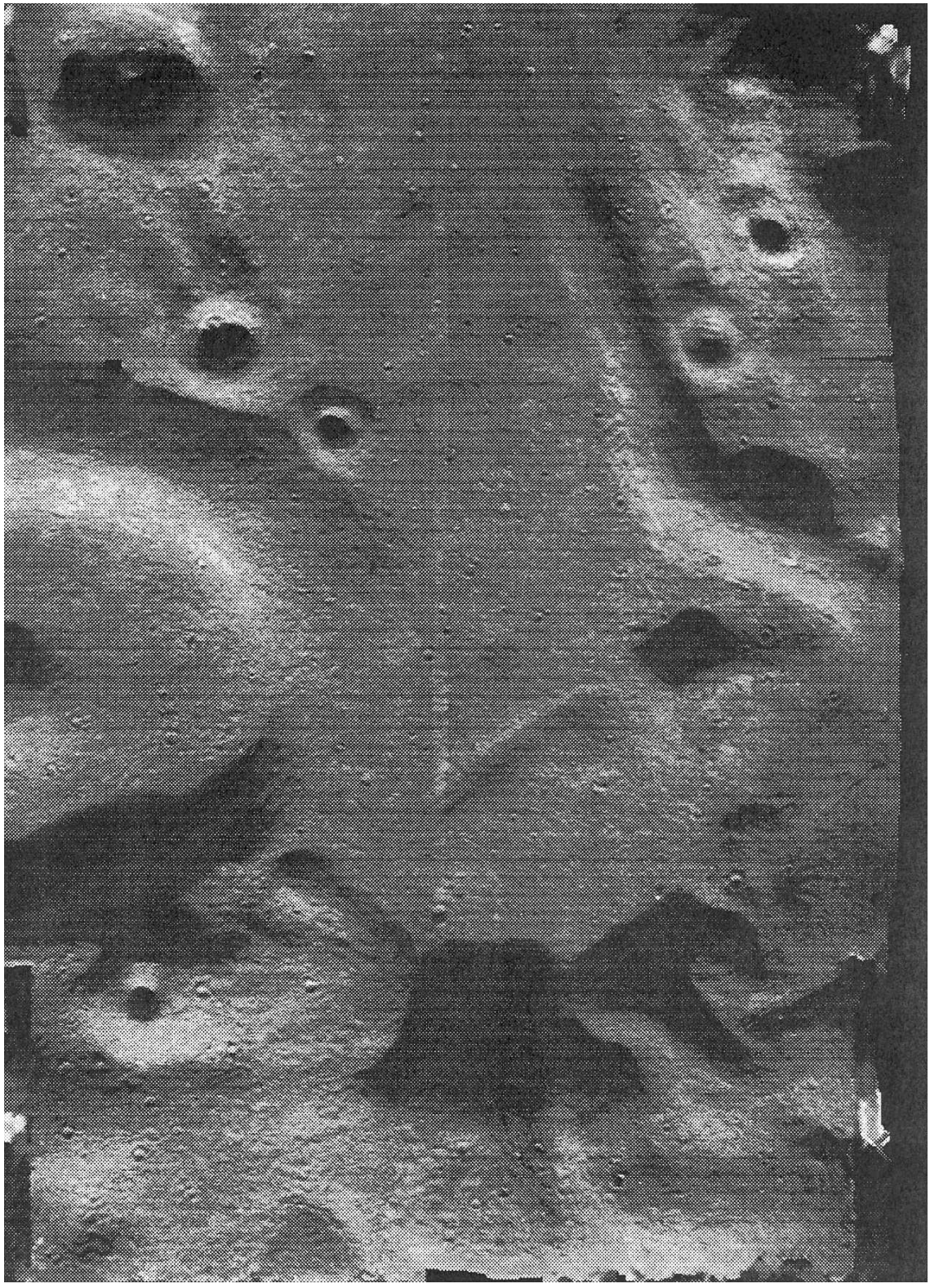

*Figure 11: Ortho image of laboratory moon mockup. Size is 1500 x 2000 mm, pixel resolution 1 mm.*

## 9.4 Calibration Accuracy

The accuracy of any calibration step is dependent on the quality of the 2D coordinates (in the images) and the quality of the 3D coordinates (on the scene). To show the effects of noise in both data sets, for each of the lander imaging configurations LA; LB and LC the results of error analysis for two different heights above ground are shown in Table 13 and Table 14.

**Major results of this evaluation are the following:**

- **For lander navigation using a DEM from orbit, the usage of a wide angle lens is preferred, since the influence of errors in 3D positions on the DEM is worse for narrow angle lenses.**
- **Expected position errors in x and y are about the same as the 3D landmark point errors. Errors in z are 1/5 of the 3D point error on the DEM.**

## 9.5 Self - Calibration

Self - Calibration of a stereo setup is needed if no reference points on the surface for calibration are known. In that case, the relative orientation of the cameras with respect to each other can be obtained using a set of corresponding points from the disparity map. To get a world coordinate calibration, one of the camera provides the reference coordinate system, at least one absolute measurement has to be performed (3D distance between scene points that are identified in both images, distance measurement between one camera and the scene, or distance measurement between the cameras). gives figures about the expected errors during self - calibration dependent on average disparity errors.

| **Disparity error** | **0,2** | **0,4** | **0,7** | **1,0** |
|---|---|---|---|---|
| **dist. = 15km $\Delta z$ = 200m** | | | | |
| **A** | 13,762 | 27,524 | 48,167 | 68,810 |
| **B** | 2,609 | 5,218 | 9,131 | 13,045 |
| **C** | 3,451 | 6,902 | 12,079 | 17,256 |
| **D** | 1,726 | 3,451 | 6,040 | 8,628 |
| **dist.=200m $\Delta z$ = 30m** | | | | |
| **LA** | 0,032 | 0,063 | 0,111 | 0,158 |
| **LB** | 0,016 | 0,032 | 0,055 | 0,077 |
| **LC** | 0,008 | 0,017 | 0,030 | 0,042 |

*Table 12: Expected self-calibration errors depending on noise in disparities (translation in meters) for the different sensor options. $\Delta z$ is the 1-sigma variation in terrain elevation.*

**These results show that the orbiter sensor options B, C and D allow a self-calibration accuracy of less than 10 meters. The errors of self-calibration for the lander motion stereo case are not significant in comparison with the reconstruction errors.**

| LA (f=10 mm, 512 x 512 pixels) | | | | | |
|---|---|---|---|---|---|
| **disp. error** | **0,0 pixels** | **0,2 pixels** | **0,4 pixels** | **0,7 pixels** | **1,0 pixels** |
| **x/y error:** | | | | | |
| **0,0** | 0,0000 | 1,4871 | 2,9742 | 5,2048 | 7,4355 |
| **0,5** | 0,7714 | 1,6753 | 3,0726 | 5,2617 | 7,4754 |
| **1,0** | 1,5428 | 2,1428 | 3,3505 | 5,4287 | 7,5938 |
| **2,0** | 3,0856 | 3,4252 | 4,2856 | 6,0507 | 8,0503 |
| **4,0** | 6,1711 | 6,3478 | 6,8504 | 8,0730 | 9,6627 |
| **8,0** | 12,3422 | 12,4315 | 12,6955 | 13,3948 | 14,4089 |
| **z error:** | | | | | |
| **0,0** | 0,0000 | 0,2097 | 0,4193 | 0,7338 | 1,0483 |
| **0,5** | 0,1092 | 0,2364 | 0,4333 | 0,7419 | 1,0540 |
| **1,0** | 0,2183 | 0,3027 | 0,4728 | 0,7656 | 1,0708 |
| **2,0** | 0,4367 | 0,4844 | 0,6054 | 0,8539 | 1,1356 |
| **4,0** | 0,8733 | 0,8981 | 0,9688 | 1,1407 | 1,3644 |
| **8,0** | 1,7466 | 1,7592 | 1,7963 | 1,8945 | 2,0371 |
| **LB (f=20 mm, 1024 x 1024 pixels)** | | | | | |
| **disp. error** | **0,0 pixels** | **0,2 pixels** | **0,4 pixels** | **0,7 pixels** | **1,0 pixels** |
| **x/y error:** | | | | | |
| 0,0 | 0,0000 | 0,7435 | 1,4871 | 2,6024 | 3,7177 |
| 0,5 | 0,7714 | 1,0714 | 1,6753 | 2,7143 | 3,7969 |
| 1,0 | 1,5428 | 1,7126 | 2,1428 | 3,0253 | 4,0251 |
| 2,0 | 3,0856 | 3,1739 | 3,4252 | 4,0365 | 4,8314 |
| 4,0 | 6,1711 | 6,2158 | 6,3478 | 6,6974 | 7,2045 |
| 8,0 | 12,3422 | 12,3645 | 12,4315 | 12,6136 | 12,8900 |
| **z error:** | | | | | |
| 0,0 | 0,0000 | 0,1048 | 0,2097 | 0,3669 | 0,5242 |
| 0,5 | 0,1092 | 0,1513 | 0,2364 | 0,3828 | 0,5354 |
| 1,0 | 0,2183 | 0,2422 | 0,3027 | 0,4270 | 0,5678 |
| 2,0 | 0,4367 | 0,4491 | 9,4844 | 0,5703 | 0,6822 |
| 4,0 | 0,8733 | 0,8796 | 0,8981 | 0,9473 | 1,0185 |
| 8,0 | 1,7466 | 1,7498 | 1,7592 | 1,7845 | 1,8236 |
| **LC (f=40 mm, 512 x 512 pixels)** | | | | | |
| **disp. error** | **0,0 pixels** | **0,2 pixels** | **0,4 pixels** | **0,7 pixels** | **1,0 pixels** |
| **x/y error:** | | | | | |
| 0,0 | 0,0000 | 0,5862 | 1,1725 | 2,0518 | 2,9312 |
| 0,5 | 1,2036 | 1,3388 | 1,6803 | 2,3788 | 3,1686 |
| 1,0 | 2,4071 | 2,4775 | 2,6775 | 3,1630 | 3,7929 |
| 2,0 | 4,8143 | 4,8498 | 4,9550 | 5,2333 | 5,6364 |
| 4,0 | 9,6286 | 9,6464 | 9,6997 | 9,8448 | 10,0648 |
| 8,0 | 19,2571 | 19,2661 | 19,2928 | 19,3661 | 19,4789 |
| **z error:** | | | | | |
| 0,0 | 0,0000 | 0,0671 | 0,1342 | 0,2348 | 0,3355 |
| 0,5 | 0,1381 | 0,1536 | 0,1926 | 0,2724 | 0,3628 |
| 1,0 | 0,2762 | 0,2843 | 0,3071 | 0,3626 | 0,4346 |
| 2,0 | 0,5525 | 0,5565 | 0,5686 | 0,6003 | 0,6464 |
| 4,0 | 1,1050 | 1,1070 | 1,1131 | 1,1297 | 1,1548 |
| 8,0 | 2,2100 | 2,2110 | 2,2140 | 2,2224 | 2,2353 |

*Table 13: Position errors dependent on 2D and 3D reference points errors and disparity errors (5000 m distance). Deviation in elevations is 100 m.*

| LA (f=10 mm, 512 x 512 pixels) | | | | | |
|---|---|---|---|---|---|
| **disp. error** | **0,0 pixels** | **0,2 pixels** | **0,4 pixels** | **0,7 pixels** | **1,0 pixels** |
| **x/y error:** | | | | | |
| **0,0** | 0,0000 | 0,1972 | 0,3944 | 0,6902 | 0,9860 |
| **0,5** | 0,5318 | 0,5672 | 0,6621 | 0,8713 | 1,1202 |
| **1,0** | 1,0636 | 1,0818 | 1,1344 | 1,2679 | 1,4503 |
| **2,0** | 2,1273 | 2,1364 | 2,1635 | 2,2364 | 2,3446 |
| **4,0** | 4,2545 | 4,2591 | 4,2728 | 4,3101 | 4,3673 |
| **8,0** | 8,5090 | 8,5113 | 8,5182 | 8,5370 | 8,5660 |
| **z error:** | | | | | |
| **0,0** | 0,0000 | 0,0384 | 0,0769 | 0,1345 | 0,1922 |
| **0,5** | 0,1051 | 0,1119 | 0,1302 | 0,1707 | 0,2191 |
| **1,0** | 0,2102 | 0,2137 | 0,2238 | 0,2496 | 0,2848 |
| **2,0** | 0,4204 | 0,4222 | 0,4274 | 0,4414 | 0,4623 |
| **4,0** | 0,8409 | 0,8418 | 0,8444 | 0,8516 | 0,8626 |
| **8,0** | 1,6818 | 1,6822 | 1,6835 | 1,6871 | 1,6927 |
| **LB (f=20 mm, 1024 x 1024 pixels)** | | | | | |
| **disp. error** | **0,0 pixels** | **0,2 pixels** | **0,4 pixels** | **0,7 pixels** | **1,0 pixels** |
| **x/y error:** | | | | | |
| 0,0 | 0,0000 | 0,0986 | 0,1972 | 0,3451 | 0,4930 |
| 0,5 | 0,5318 | 0,5409 | 0,5672 | 0,6340 | 0,7252 |
| 1,0 | 1,0636 | 1,0682 | 1,0818 | 1,1182 | 1,1723 |
| 2,0 | 2,1273 | 2,1295 | 2,1364 | 2,1551 | 2,1836 |
| 4,0 | 4,2545 | 4,2557 | 4,2591 | 4,2685 | 4,2830 |
| 8,0 | 8,5090 | 8,5096 | 8,5113 | 8,5160 | 8,5233 |
| **z error:** | | | | | |
| 0,0 | 0,0000 | 0,0192 | 0,0384 | 0,0673 | 0,0961 |
| 0,5 | 0,1051 | 0,1069 | 0,1119 | 0,1248 | 0,1424 |
| 1,0 | 0,2102 | 0,2111 | 0,2137 | 0,2207 | 0,2311 |
| 2,0 | 0,4204 | 0,4209 | 0,4222 | 0,4258 | 0,4313 |
| 4,0 | 0,8409 | 0,8411 | 0,8418 | 0,8436 | 0,8464 |
| 8,0 | 1,6818 | 1,6819 | 1,6822 | 1,6831 | 1,6845 |
| **LC (f=40 mm, 512 x 512 pixels)** | | | | | |
| **disp. error** | **0,0 pixels** | **0,2 pixels** | **0,4 pixels** | **0,7 pixels** | **1,0 pixels** |
| **x/y error:** | | | | | |
| 0,0 | 0,0000 | 0,0698 | 0,1396 | 0,2444 | 0,3491 |
| 0,5 | 0,7384 | 0,7417 | 0,7515 | 0,7778 | 0,8168 |
| 1,0 | 1,4769 | 1,4785 | 1,4834 | 1,4969 | 1,5176 |
| 2,0 | 2,9537 | 2,9545 | 2,9570 | 2,9638 | 2,9743 |
| 4,0 | 5,9074 | 5,9079 | 5,9091 | 5,9125 | 5,9177 |
| 8,0 | 11,8149 | 11,8151 | 11,8157 | 11,8174 | 11,8200 |
| **z error:** | | | | | |
| 0,0 | 0,0000 | 0,0384 | 0,0769 | 0,1345 | 0,1922 |
| 0,5 | 0,4076 | 0,4094 | 0,4148 | 0,4292 | 0,4506 |
| 1,0 | 0,8151 | 0,8160 | 0,8188 | 0,8262 | 0,8375 |
| 2,0 | 1,6303 | 1,6307 | 1,6321 | 1,6358 | 1,6416 |
| 4,0 | 3,2606 | 3,2608 | 3,2615 | 3,2633 | 3,2662 |
| 8,0 | 6,5211 | 6,5212 | 6,5216 | 6,5225 | 6,5239 |

*Table 14: Position errors dependent on 2D and 3D reference point errors and disparity errors (200 m distance). Deviation in elevations is 30 m.*

## 9.6 Tracking of Crater Rim - Experiments

### *9.6.1 General Remarks*

The morphology of the Southpole region on the Moon is dominated by flat craters with a diameter in the range between 20 and 200 kilometers. In between these larger structures hundreds of smaller sized craters are dispersed all over the surface. The rims of the larger craters are broad and curved, seldom can a sharp edge between crater floor and the surrounding of the crater be detected. In this sense the big impact structure used by JOANNEUM RESEARCH for the simulations Figure 11 is similar to the real Moon surface. The smaller the crater become, the sharper the crater rims (20 km and below).

This observation leads to the conclusion, that for landing purposes smaller craters are somewhat better suited because the crater rim is much better defined than for the bigger ones. This is in contradiction to the fact that on a small crater a landing spot can hardly be found. In addition, since the rims of those craters bend a little up before the actual depressions begin, a landing spot on such a structure would most probably not allow the view into the crater itself! From the current knowledge of morphology on the Moon's South Pole region, a landing spot on a medium sized crater (50 km - 100 km) seems to be most reasonable from the computer vision point of view. In this case, the crater rim is relatively well defined under flat illumination, and the chance to find a reasonable landing spot seems to be high enough for a successful operation.

### *9.6.2 Specific observations:*

Specific experiments have been undertaken to estimate the behavior of the Moon's surface under different illumination conditions.

1. In the first set of experiments a flat illumination with about 6 degrees vertical angle has been simulated (Figure 12). The first obvious observation is, that a large amount of the surface (about 50%) is cast into shadows. This means that the generation of elevation models will result in DEMs with undefined areas at the shadows (See also Table 11). After a change of illumination 30 degrees horizontally, the second specific property of the Moon's surface under such flat incident angles for the light becomes clear: The long shadows move around the surface, and so the image content changes quite drastically. The crater rims seem to be relatively well defined in the images.
2. The second set of experiments was undertaken with a vertical illumination angle of 13 degrees (Figure 13) and three different horizontal angles. In all the images the crater rim was as well defined as in the 6° images. The horizontal displacement of the light source by far did not change the surface properties as much as in the first experiment. Because of the steeper incident angle of the light, the shadowy regions were substantially smaller than in the 6deg images.

The conclusion of the previous two experiments is, that as steep as possible an incident angle for the light is to be obtained the surface behaves much more friendly for any processing algorithms described in this report.

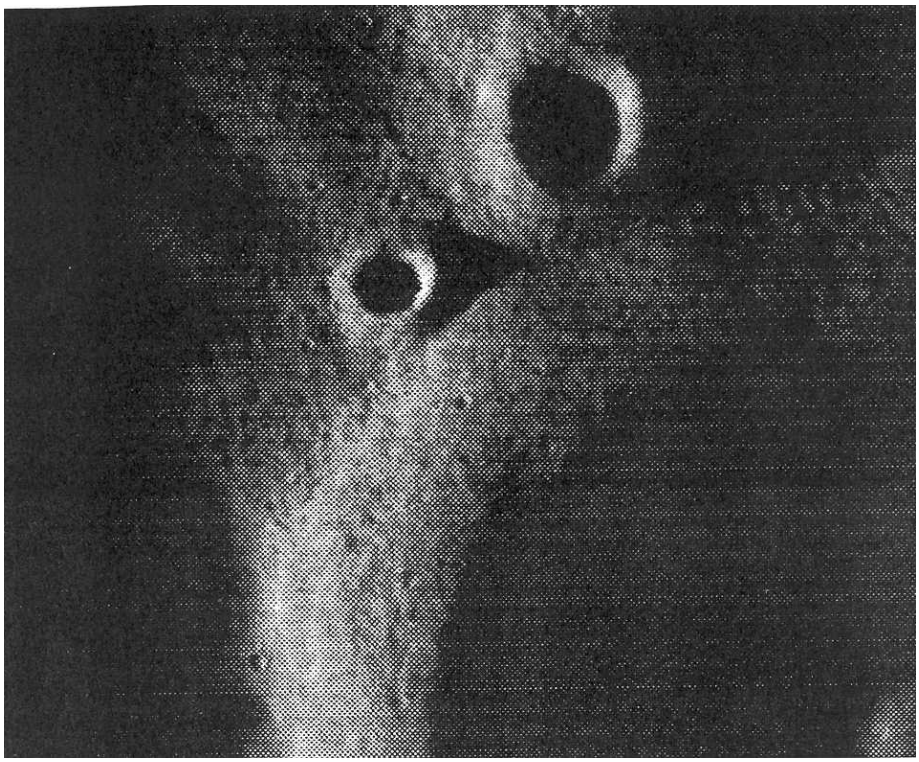

*Figure 12: Crater rim illuminated with 6 degrees angle*

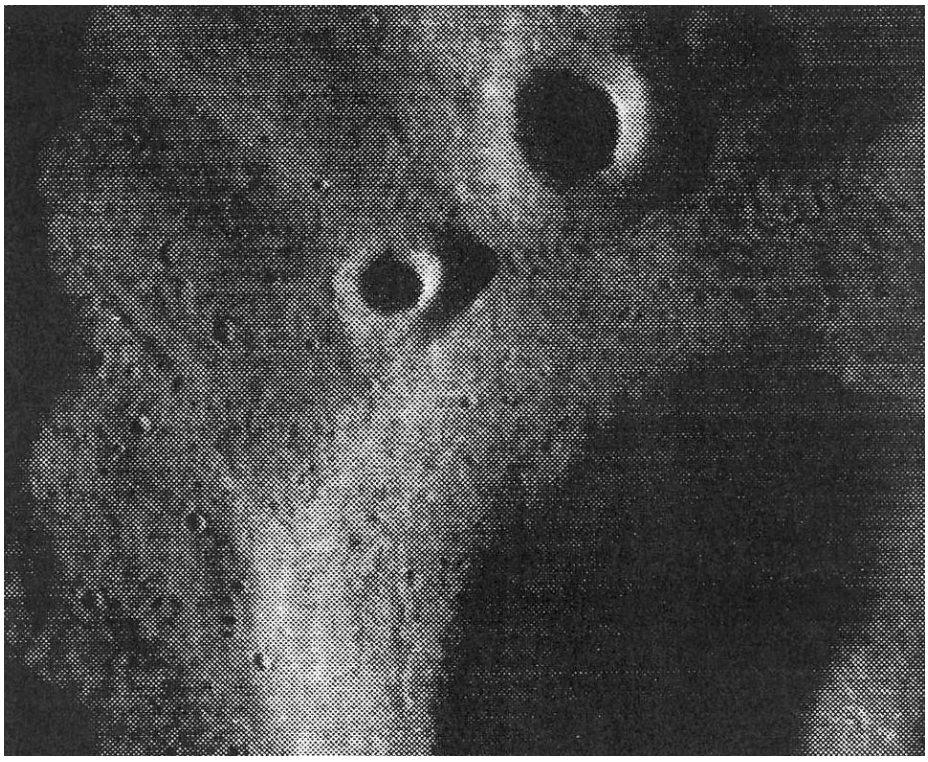

*Figure 13: Crater rim illuminated with 13 degrees angle*

## 9.7 Errors During Position Initialization

### *9.7.1 Accuracy*

Using landmarks on a precalculated ortho image (from orbiter), the calculation of the first spacecraft position during descent is an important step for absolute navigation. Both artificially rendered images and practical experiments were performed. In all cases it is assumed that the resolution of the orbiter image is at least as fine as the lander image. The MOON mockup ortho image with 1mm pixel resolution was used for the experiments. For the first lander images in the simulation a scale factor of 1:3000 resulted in a ground distance of about 5 km and a real pixel resolution of 3 m. dx,dy,dz are RMS errors from the ideal world position. Six experiments were performed to obtain the RMS error for each of the angular configurations. The results are shown in Table 15.

| | dx (mm) | dy (mm) | dz (mm) | d◆ ☎Gon ) | d↗ n) ☎Go | d& on) ☎G |
|---|---|---|---|---|---|---|
| | | & mockup images: | | | | |
| ◆ | 2.26 | 2.89 | 0.22 | 0.14 | 0.10 | 0.01 |
| ◆ | 2.68 | 3.10 | 0.60 | 0.20 | 0.22 | N.a. |
| ◆ | 2.30 | 2.20 | 0.58 | 0.27 | 0.21 | N.a. |
| ◆ | 5.01 | 5.80 | 1.75 | 0.20 | 0.58 | N.a. |
| | | ◆ rendered images: | | | | |
| & | 1.08 | 0.71 | 0.12 | 0.03 | 0.05 | 0.007 |
| & | 1.74 | 2.49 | 0.22 | 0.11 | 0.08 | 0.006 |

*Table 15: RMS errors of position initialization, DEM resolution 1 mm/pixel (SCALE = 1:3000)*
*Scene distance 1700 mm, 500x700 pixel camera, focal length = 14 mm*

| | dx (mm) | dy (mm) | dz (mm) | d◆ ☎Gon ) | d↗ n) ☎Go | d& on) ☎G |
|---|---|---|---|---|---|---|
| | | & mockup images: | | | | |
| ◆ | 3.54 | 4.63 | 0.33 | 0.21 | 0.15 | 0.013 |
| ◆ | 3.90 | 5.43 | 0.96 | 0.18 | 0.16 | 0.022 |
| ◆ | 3.54 | 4.70 | 0.73 | 0.41 | 0.15 | 0.044 |
| ◆ | Failed | | | | | |
| | | ◆ rendered images: | | | | |
| & | 1.86 | 3.00 | 0.38 | 0.13 | 0.08 | 0.014 |
| & | 4.64 | 4.10 | 0.35 | 0.18 | 0.20 | 0.015 |

*Table 16: RMS errors of position initialization, DEM resolution 2 mm/pixel (SCALE = 1:3000) )*
*Scene distance 1700 mm, 500x700 pixel camera, focal length = 14 mm*

| | dx (mm) | dy (mm) | dz (mm) | d◆ ☎Gon ) | d↗ n) ☎Go | d& on) ☎G |
|---|---|---|---|---|---|---|
| | | & mockup images: | | | | |
| ◆ | 3.21 | 6.08 | 0.48 | 0.29 | 0.14 | 0.020 |
| ◆ | 3.13 | 6.08 | 1.05 | 0.18 | 0.13 | 0.025 |
| ◆ | 3.69 | 4.19 | 1.54 | 0.24 | 0.14 | 0.054 |
| ◆ | Failed | | | | | |
| | | ◆ rendered images: | | | | |
| & | 2.47 | 3.66 | 0.28 | 0.18 | 0.11 | 0.020 |
| & | 6.21 | 6.02 | 0.91 | 0.25 | 0.29 | 0.026 |

*Table 17: RMS errors of position initialization, DEM resolution 4 mm/pixel (SCALE = 1:3000) Scene distance 1700 mm, 500x700 pixel camera, focal length = 14 mm*

Position errors are almost compensated by errors in viewing angle. It is shown that experiments on the real mockup show larger errors than using the rendered images. This can be caused by stereo reconstruction errors of the reference DEM and errors in intrinsic calibration of the camera. A factor of three in terms of position and pointing errors can be derived as rule of thumb. (The rendered images are fully consistent with the reference DEM.)

**Major result of these experiments is that the expected position initialization error using a 3m resolution DEM and an optical sensor with 700x500 pixels (focal length = 14mm) will be below 10 meters in x and y, and below 3 meters in z.**

### *9.7.2 Robustness*

The robustness of position initialization was investigated in terms of changes in illumination direction. The experiments showed that horizontal illumination changes up to 20 degrees can be tolerated, although the accuracy decreases depending on the amount of change. The coarse position of the first lander image was always correctly located within the EU image, but the matching necessary for calibration failed because of different shapes caused by the changed shadow locations.

Changing vertical illumination angle from 30 to 20 degrees caused a failure rate of almost 100 percent. This means that the reference DEM has to be acquired in the same season as given during landing, but incidence angle changes caused by different time of day may vary up to 20 degrees.

## 9.8 Tracking Errors

### *9.8.1 Influence of Position Initialization*

The accuracy of landmark tracking is highly dependent on errors in the first position as a result from the position initialization process (Section 9.7.1). Figure 14 shows the results (position errors on a path consisting of 10 images) using rendered images for three different initial error sets. It is shown that the position initialization errors are almost directly projected on the tracking errors.

**This means that tracking does not become unstable even if the first position suffers from a relatively high error**.

On Figure 15 the dependency between the first position error and the last position error is displayed as a function.

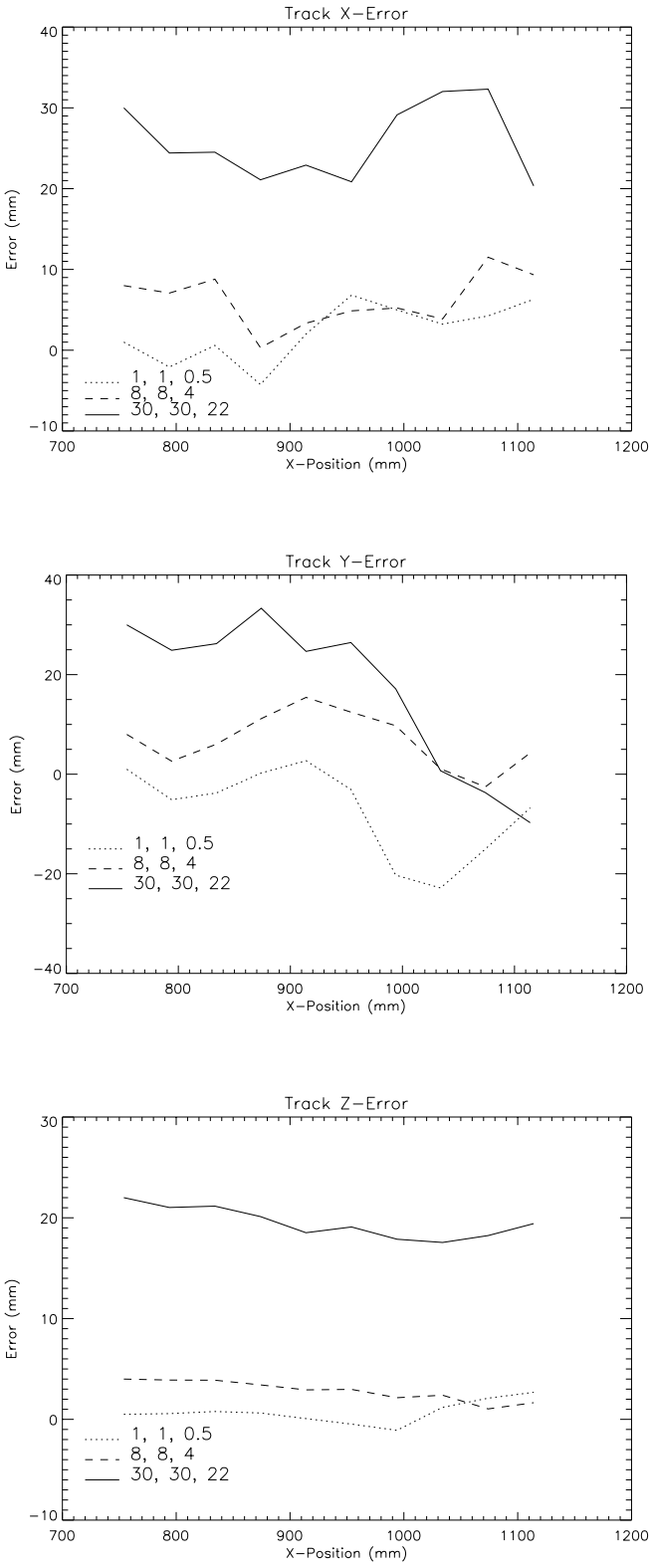


Figure 14: Tracking errors (path) depending on position initialization errors (1, 8 and 30 mm in x/y and 0.5, 4 and 22 mm in z)

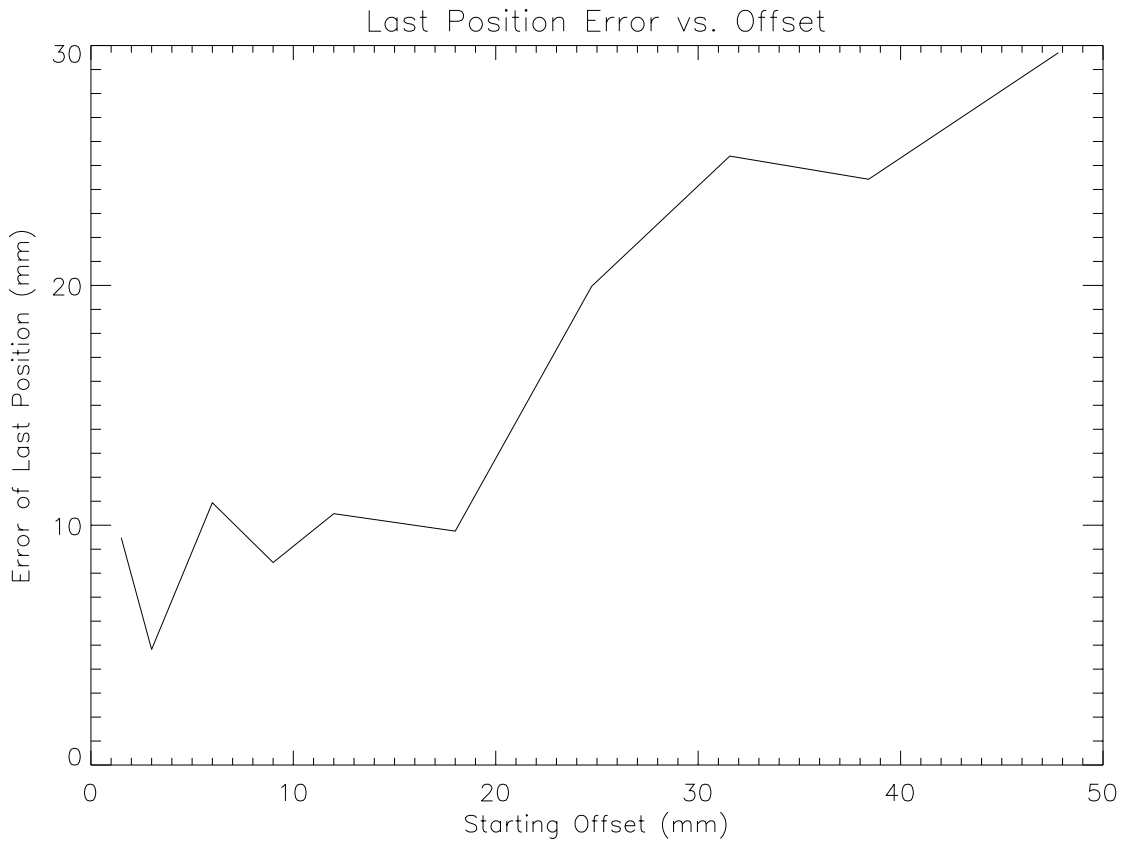


*Figure 15: Tracking errors (last positions after 10) depending on position initialization errors*

## *9.8.2 Tracking Robustness Depending on Number of Positions*

The following experiments were performed for two different vision sensor properties: Having a predefined path, the image acquisition frequency was varied between 80 and 10 frames for the whole path. Three of the used frames (first, middle and last) are shown in frame Figure 16 and Figure 17 show the position errors of each configuration. *A pointing noise in the range of +/- 2 Gon was added during rendering*. All experiments show that a lower number of positions leads to a better result, although tracking converges to the right solution at the end of the path, regardless of the imaging frequency. This effect could be observed throughout all tracking experiments in the framework of this study.

**The major result of these experiments is that the number of images used for tracking is not a crucial parameter and the pointing noise can be up to +/- 2 Gon**

.

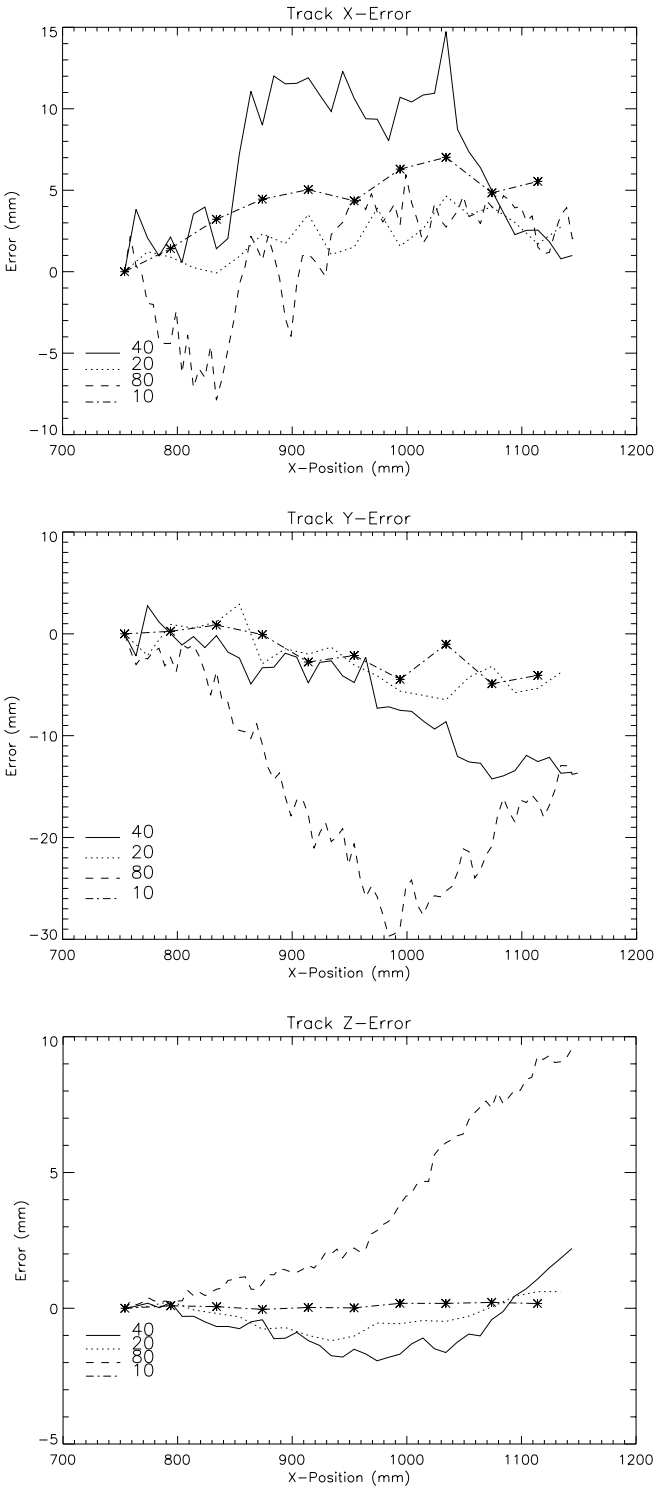


*Figure 16: Tracking errors depending on number of acquired images. The path marked with an asterisk (*) has been selected adaptively (Distance between image acquisition depending on scene distance). The other paths use equal distances between the image acquisition positions.*

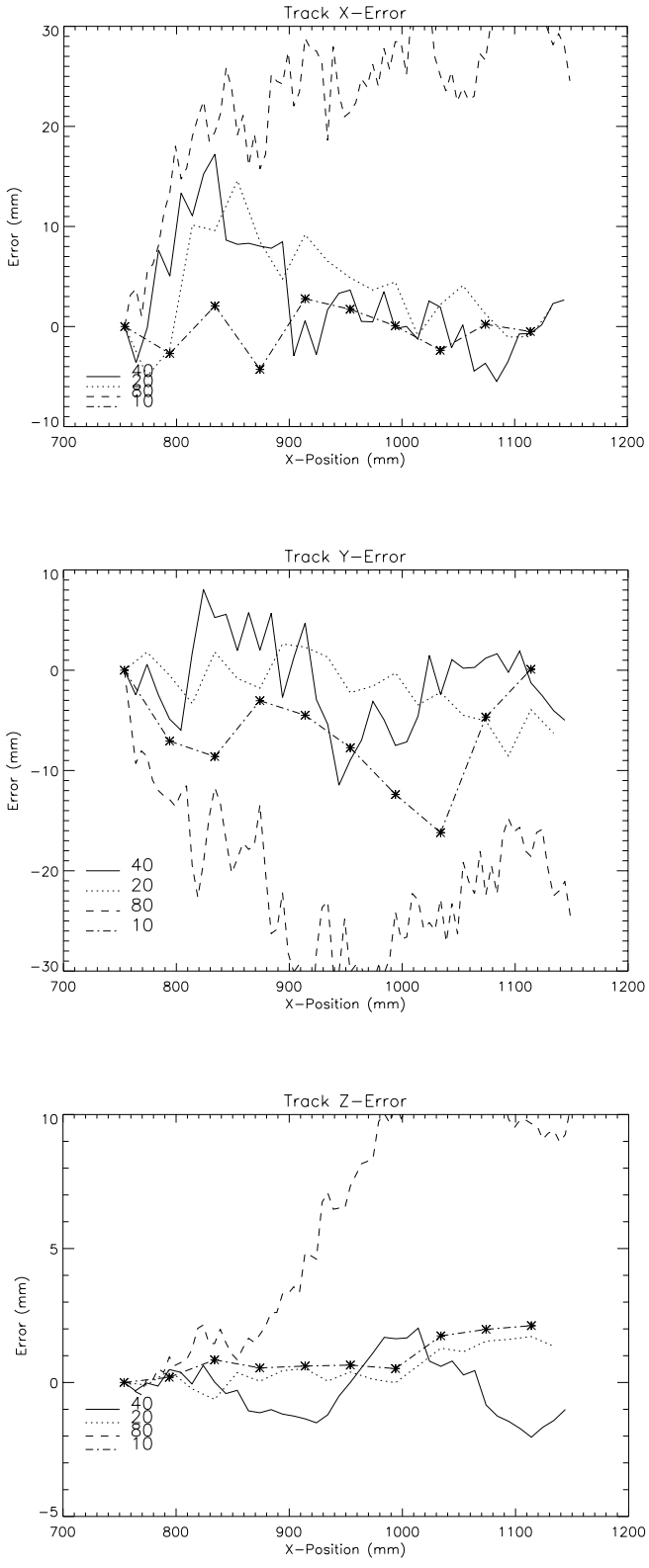


*Figure 17: Tracking errors depending on number of acquired images: Half resolution images*

### *9.8.3 Tracking Robustness Depending on Algorithmic Parameters*

The major parameters during landmark tracking are the number of landmarks („Interest points“ in the algorithmic terminology), and their backprojection error as a

measure of the calibration consistency. The results on Figure 18 show that **the optimum number of landmarks is at about 500 points, backprojection threshold is not a crucial factor for tracking. However, a smaller set of landmarks (>200) still leads to robust tracking**.

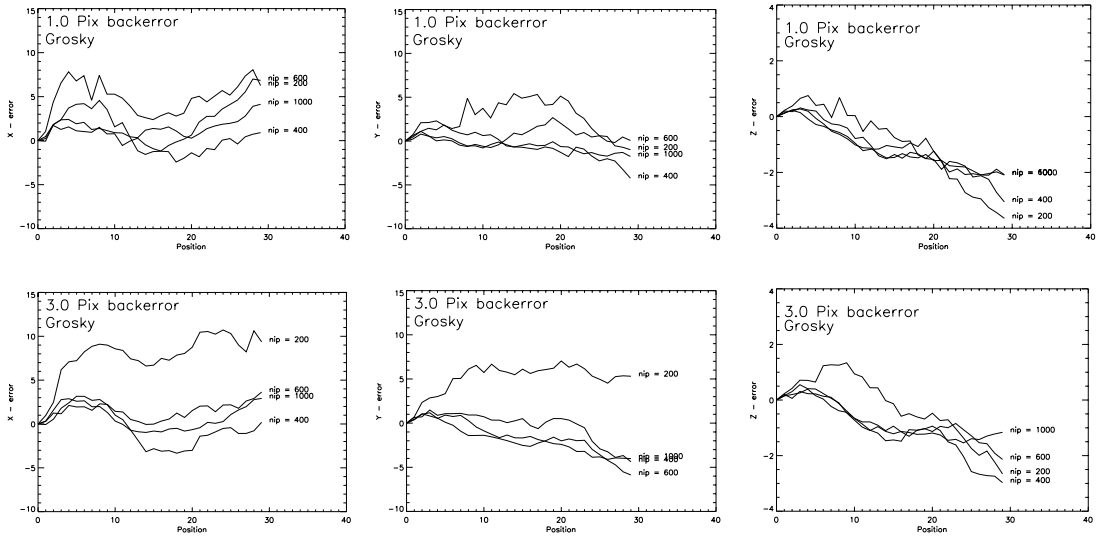


*Figure 18: Tracking accuracy using different number of landmarks (nip = 200 .. 1000) and different backprojection threshold (calibration consistency)*

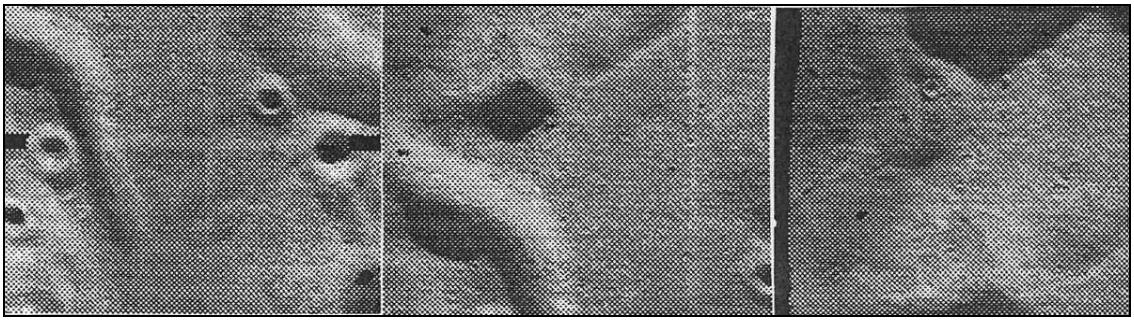

*Figure 19: First, second and last frame of tracking robustness experiment*

## 9.9 Lateral Motion Measurement Errors

Real mockup images were used to verify the functionality of lateral motion measurement using landmark tracking together with self-calibration. The process showed instability mainly in horizontal direction (error 5 % of range after 10 measurements). These errors are well compensated by pointing errors, which means that updating the pointing values by other sensors could lead to significant improvement.

**Unlike tracking, the lateral motion measurement without reference DEM should be performed with update frequency as low as possible.**

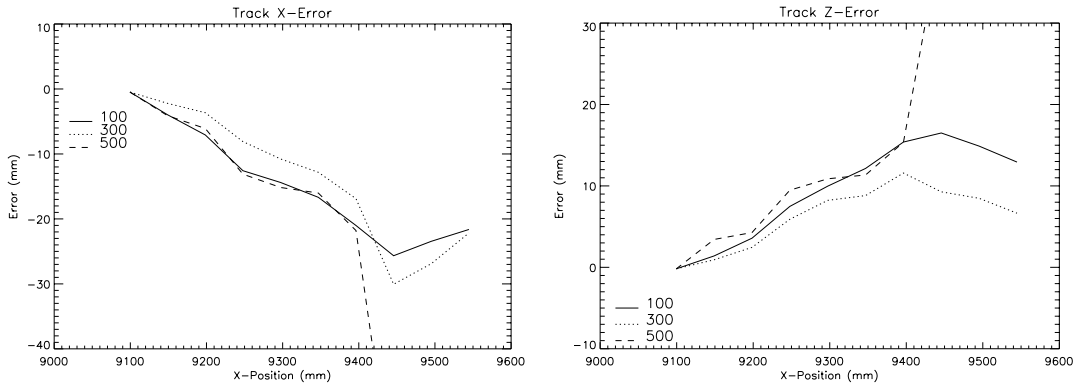


*Figure 20: Lateral motion measurement errors for **illumination angle of 35 degrees** on mockup: Number of positions is 10, number of landmarks is 100,300 and 500. Range of motion in (x,y,z) is (500,500,1000mm) corresponding to a descent angle of about 35 degrees to vertical.*

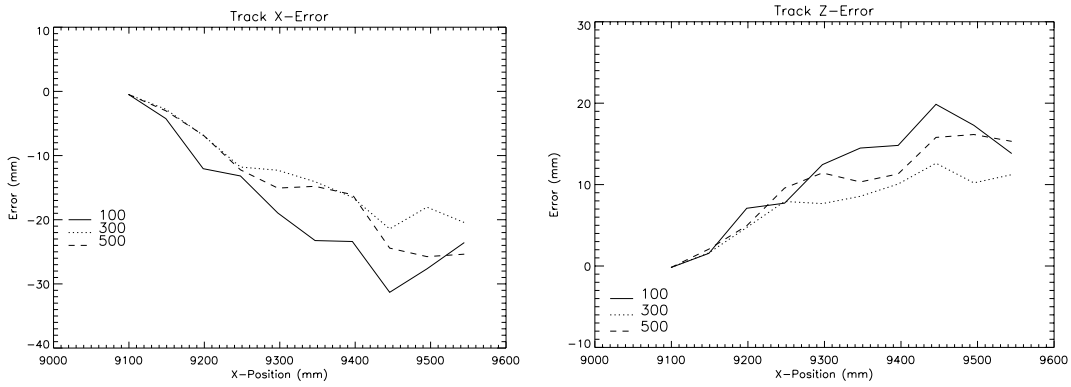


*Figure 21: Lateral motion measurement errors for **illumination angle of 13 degrees** on mockup: Number of positions is 10, number of landmarks is 100,300 and 500. Range of motion in (x,y,z) is (500,500,1000mm) corresponding to a descent angle of about 35 degrees to vertical.*

## 9.10 Obstacle Detection Errors

To verify the 2D obstacle detection identified as low-complexity strategy for the late landing phase, a separate mockup was constructed. A scale factor of 1:200 was assumed leading to an obstacle size of 2.5 mm for a half-meter obstacle in reality. For one of the distances the illumination was varied.

Three classes of sizes, each of them containing 20 manually measured test samples and two different distances to ground were investigated.

Table 18 shows the results. In this simple test, the influence of illumination direction is not significantly high, although flat illumination caused some more misdetections. **A detection rate of 95 % for 60-100cm obstacles from 100 m distance and a detection rate of 80-90 % for 1-1.5m obstacles from 250 m distance could be found.**

| Obstacle size | 0.3m - 0.6m | 0.6m - 1m | 1m - 1.5m |
|---|---|---|---|
| 250 m distance, 23° illumination | | 12 | 18 |
| 250 m distance, 12° illumination | | 9 | 16 |
| 100 m distance, 12° illumination | 15 | 19 | |

*Table 18: Obstacle recognition rate depending on distance and illumination. Number of obstacles was 20 in each class. Simulation on real mockup with scale 1:200, focal length of camera 14 mm, 572x700 pixels*

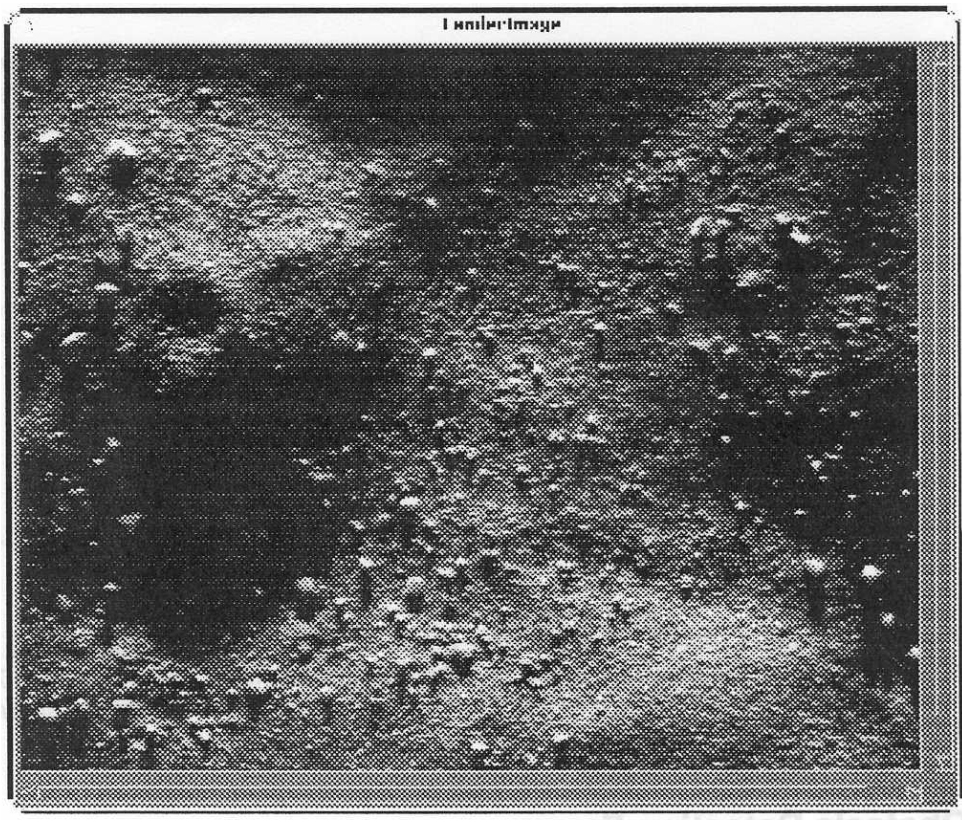

*Figure 22: Input image for obstacle detection test: 100 m distance*

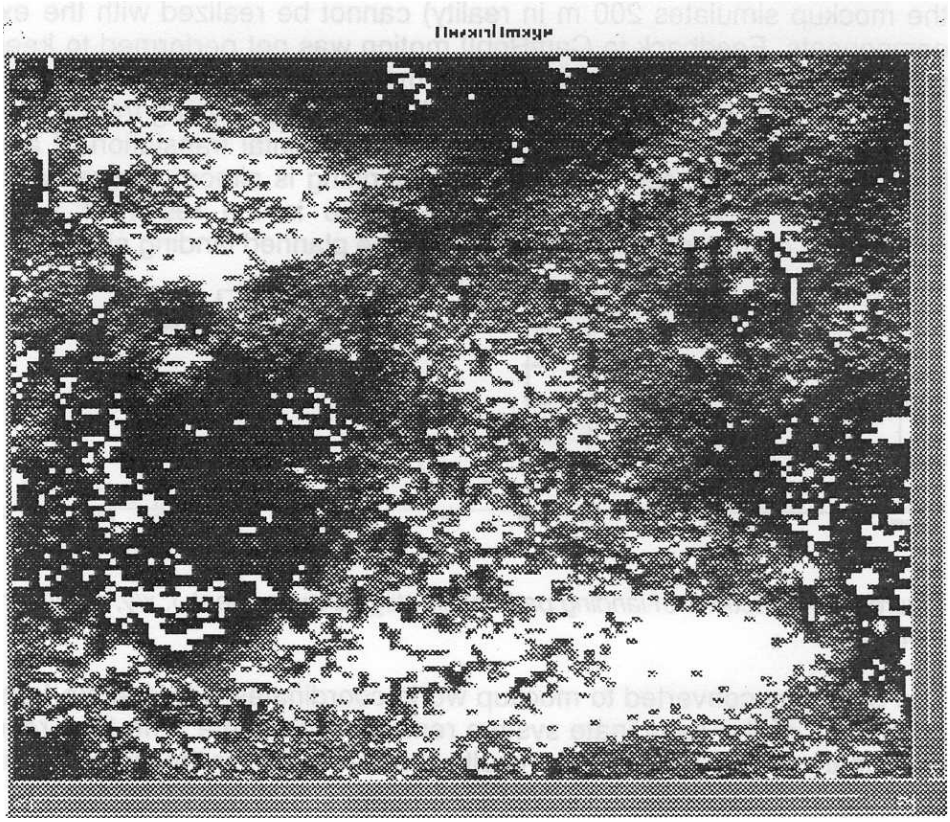

*Figure 23: Obstacle detection test: Hazardous areas marked.*

# 10 CLOSED LOOP EXAMPLE

To show the functionality of the closed loop, this section gives an example of the data and results acquired during a whole chain of one landing procedure. Hazard avoidance was excluded in this chain since the required range (6 cm distance from the mockup simulates 200 m in reality) cannot be realized with the existing optical components. Feedback to CamRobII motion was not performed to keep the original path. The landing path (Figure 24) was made available by J. de Lafontaine (ESTEC) as a result of a software simulation of the landing beginning from a ground distance of 5km (1.7 m in the mockup). It shows a horizontal translation of about 700 m in both directions. Descent angle at the beginning is almost vertical. At an altitude of about 1000 m a horizontal hovering phase is the result of a simulated late recognition of the position with respect to the planned landing site.

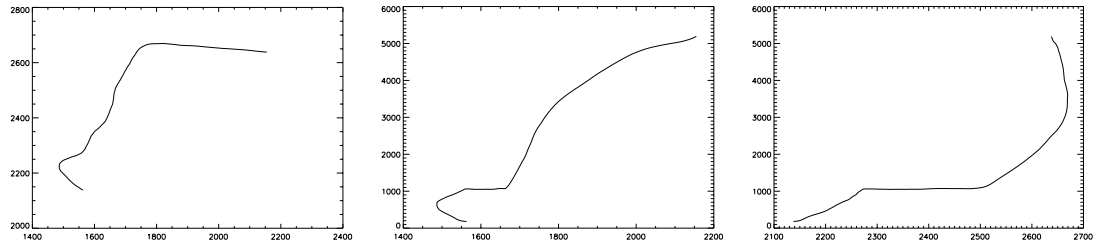


*Figure 24: Projections of landing path for Strategy 2 experiment. l: x/y, m: x/z, r: y/z, values in meters*

The path was converted to mockup world coordinates with a scale factor of 1:3000, orientation of the coordinate system remained the same. The time resolution of the coordinates is 2 seconds. This results in 284 images for the whole sequence.

## 10.1 DEM Generation

The global DEM was acquired using CamRobII, a high accuracy camera positioning device. 8 stereo configurations (hence 16 images) were calibrated and matched, the resulting DEMs and ortho images were merged to get the result depicted on Figure 10 and Figure 11. A ground resolution of 1 mm corresponding to 3m in reality has been obtained.

## 10.2 Position Initialization

The first image of the sequence is shown in Figure 25, the last of the frames used for tracking is shown in Figure 28. A comparison of the positions fed into the CamRobII motion sequence with the result of the position initialization algorithm is shown in Table 19. The errors are well within the values found during experimentation. Multiplying the scale factor leads to a position error of 5 meters in y and 3 meters in x and z.

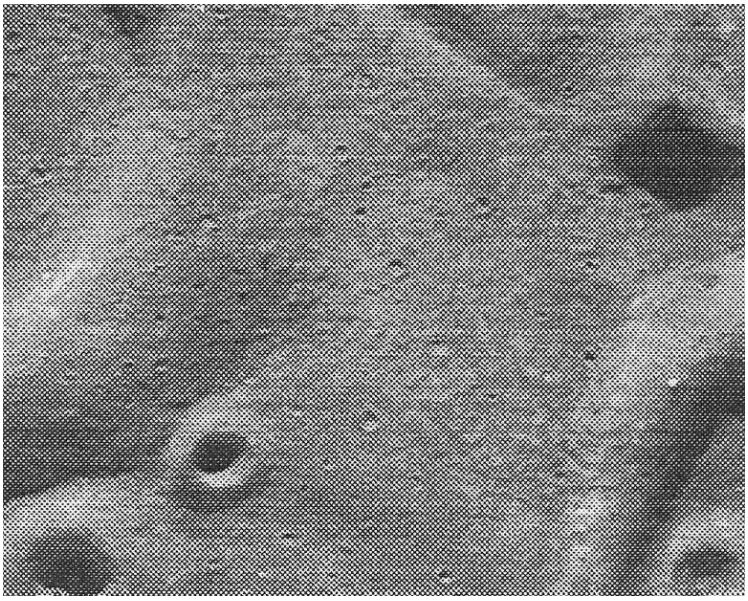

*Figure 25: First image of mockup landing, used for position initialization*

| | x (mm) | y (mm) | z (mm) | ◆☎Gon) | ✗☎Gon) | &☎Gon) |
|---|---|---|---|---|---|---|
| Reference | 715.00 | 879.67 | 1713.47 | 0 | 0 | 0 |
| Posinit result | 716.10 | 881.45 | 1712.42 | -0.06 | 0.04 | 0.23 |
| **Difference** | 1.10 | 1.78 | 1.05 | 0.06 | 0.04 | 0.23 |

*Table 19: Position initialization result of Strategy 2 experiment*

## 10.3 Tracking

A tracking update rate of 10 seconds was assumed. Every 5th image was used to get the respective position. Figure 26 shows the tracking result of 42 frames in comparison with the path fed into the CamRobII motion interface. Zooming into the first 8 positions is shown in Figure 27. The navigation oscillates but no significant deviation from the real positions can be observed.

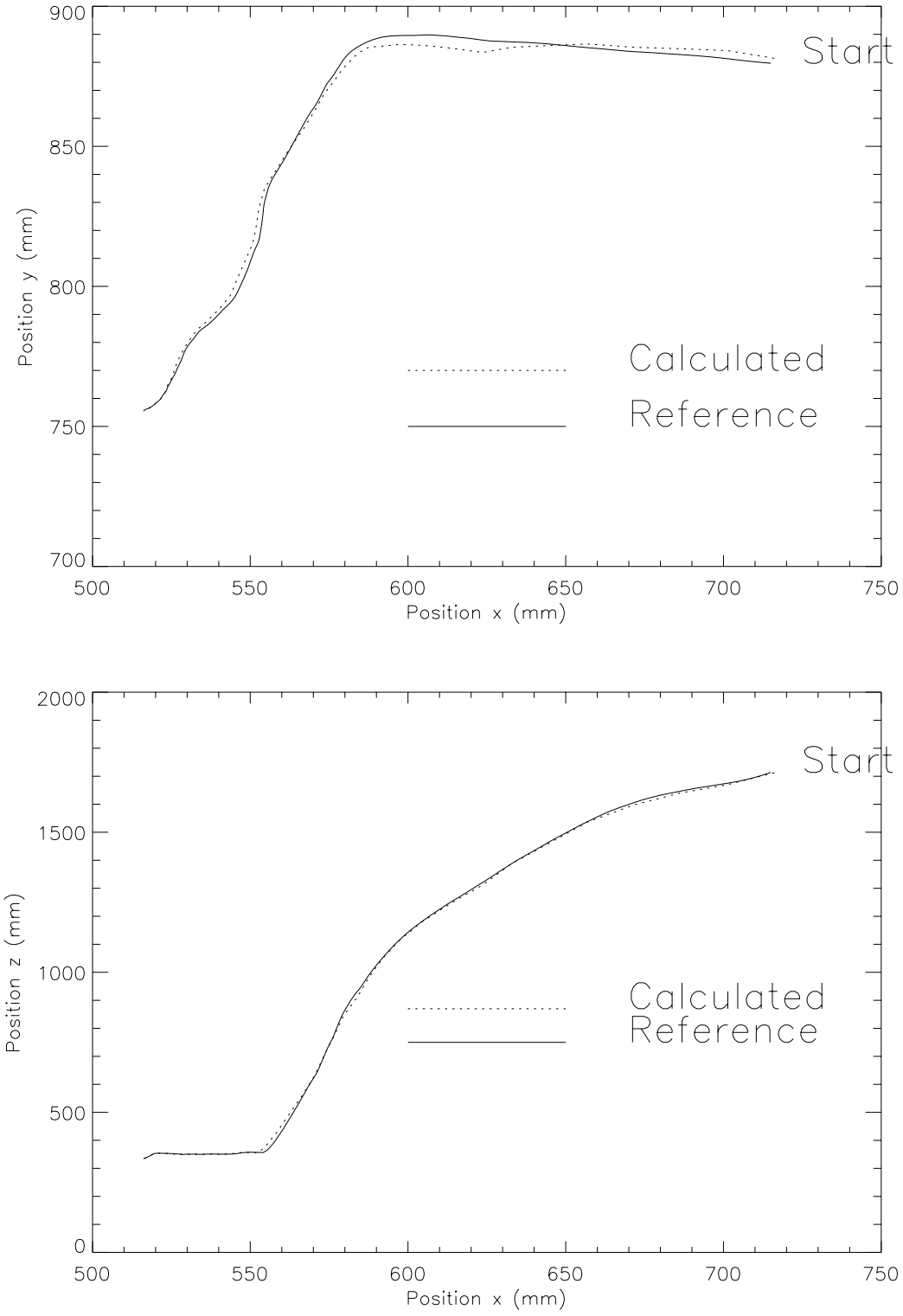


*Figure 26: Comparison between CamRobII world coordinate path and tracking result (x/y projection and x/z projection)*

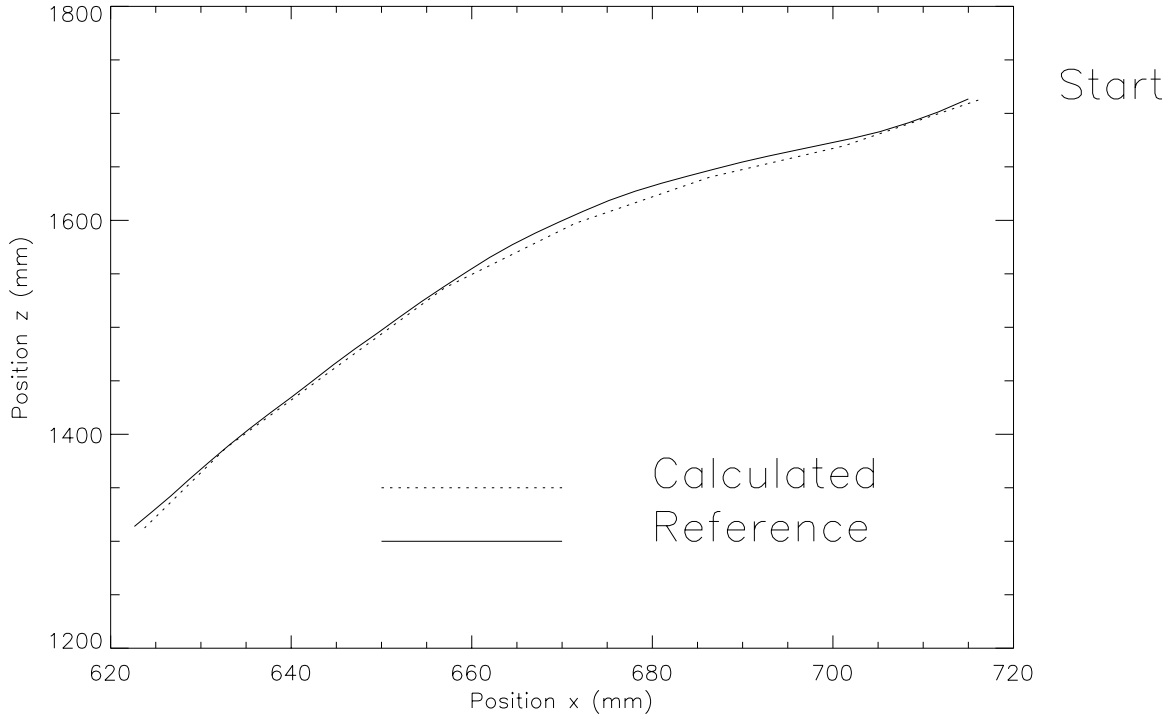


*Figure 27: First eight positions of tracking path and first 35 positions of reference path*

The tracking terminates at a ground distance of 333 mm since the CamRobII workspace overflew. **At the last position, a navigation error of less than 1 mm (corresponding to 3 m in reality) was achieved!**

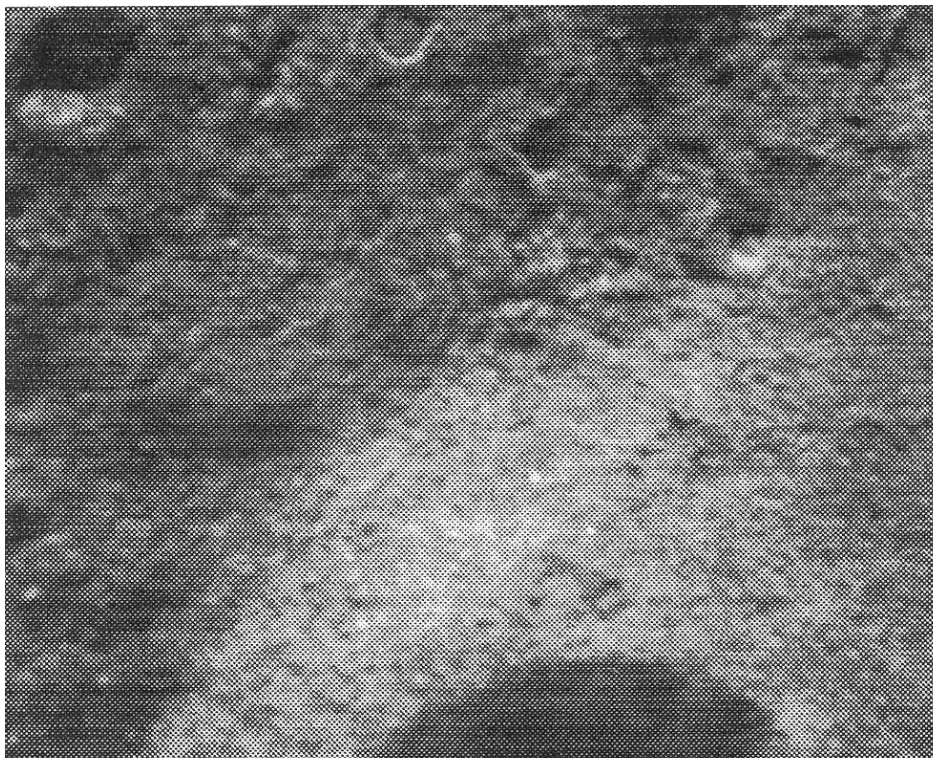

*Figure 28: Last of tracking frames for Strategy 2 experiment (ground distance 333 mm)*

# 11 ABBREVIATIONS

| | |
|---|---|
| 2D | Two - Dimensional |
| 3D | Three - Dimensional |
| DEM | Digital Elevation Model |
| EU | Ellipsis of Uncertainty |
| FOV | Field of View |
| HFVM | Hierarchical Feature Vector Matching |
| LSLS | Lander Selected Landing Site |
| MB | Mega Bytes |
| RMS | Root Mean Square |
| SOW | Statement of Work |
| SC | Spacecraft |
| SW | Software |
| WAC | Wide Angle Camera |

# 12 SUMMARY

The relevant mission parameters for an autonomous landing on the Lunar surface at the beginning of the next century were identified. A landing near the south pole was considered as baseline. An orbiting phase with a few tens of kilometers ground distance is followed by a descent from an altitude of 5 km having a horizontal velocity near zero from this moment. The same SC is used as orbiter and lander.

Different options of vision sensors and their optical components are proposed. The effect of the various options on the error behavior of the algorithms used are described by means of theoretical considerations as well as mockup experiments.

A set of computer vision strategies to support an unmanned autonomous landing near the Lunar South Pole was introduced. Important features of these strategies are listed in the following tables.

| **Mapping** from Orbiter Imagery (SC1, Page 9) | | | | |
|---|---|---|---|---|
| **Requirements from mission and sensors** | **Required Hardware (on SC)** | **Estimated Accuracy and Performance** | **Advantages, Benefits** | **Disadvantages** |
| • Orbit phase, 15-25 km ground distance at last orbit before landing<br>• Optic with 100-200 mm focal length<br>• Accurate knowledge about orbit and speed<br>• Camera pointing accuracy better than 0.3 degrees | • One CCD camera (1000 x 1000 pixels)<br>• DSP board<br>• 10 MB memory<br>• Up / downlink more than 10 Kbits / second<br>• Compression Hardware | • 3m resolution and 5m accuracy DEM of uncertainty region (EU)<br>• 1 hour processing on Earth | • Enables absolute navigation<br>• Enables landing spot selection on Earth<br>• Provides information for rover path<br>• Other areas can be mapped with same instrument (about 30000 km² for 20 days orbit)<br>• Can be started 3 orbits before touch-down | • Shadow areas cannot be mapped<br>• Self-calibration can cause problems at overlap areas |

| **Mapping** from Lander Motion Stereo (SC2, Page 12) | | | | |
|---|---|---|---|---|
| **Requirements from mission and sensors** | **Required Hardware (on SC)** | **Estimated Accuracy and Performance** | **Advantages, Benefits** | **Disadvantages** |
| • Change of horizontal motion during landing<br>• Camera pointing accuracy 2 degrees<br>• Optic with 10-20 mm focal length<br>• One distance measurement | • One CCD camera (500x500 pixels)<br>• DSP board<br>• 2 MB memory, in case of lander proc. 16 MB | • Processing takes about 10 seconds to one minute<br>• Absolute accuracy in range of distance measurement accuracy<br>• Ground and DEM resolution about 0.2m | • Processing on ground provides information for rover<br>• If processed on lander, could be used as high level hazard avoidance strategy<br>• Not dependent on orbiter DEM | • Horizontal displacement necessary<br>• High requirements to HW performance if processed on lander |

| **Mapping** from Lander Stereo Cameras (SC3, Page 15) | | | | |
|---|---|---|---|---|
| **Requirements from mission and sensors** | **Required Hardware (on SC)** | **Estimated Accuracy and Performance** | **Advantages, Benefits** | **Disadvantages** |
| • Optic with 10-20 mm focal length<br>• Camera pointing accuracy 2 degrees | • 2 cameras( 500x500 pixels)<br>• DSP board<br>• 2 MB memory, in case of lander processin g 16 MB | • Ground resolution about 0.2 m, DEM resolution about 2 m. | • Processing on ground provides information for rover<br>• If processed on lander, could be used as high level hazard avoidance strategy<br>• Not dependent on orbiter DEM<br>• Calibration can be done on ground<br>• No additional lander motions necessary | • Low accuracy because of small stereo base<br>• Physical instabilities can cause calibration problems<br>• Only applicable to last 100 meters |

| **Tracking** of Crater Rim (SC4, Page 18) | | | | |
|---|---|---|---|---|
| **Requirements from mission and sensors** | **Required Hardware (on SC)** | **Estimated Accuracy and Performance** | **Advantages, Benefits** | **Disadvantages** |
| • Optic with 10-20 mm focal length<br>• Target crater size between 50 and 100km<br>• Rough distance estimate | • camera (500x500 pixels)<br>• DSP board<br>• 2 MB memory, | • Update rate below 1 second | • Fast<br>• Can be well adopted to moon texture and illumination conditions<br>• No calibration necessary | • Only surface-relative navigation, no relation to global DEM<br>• Allows only landing on a crater rim |

| **3D Position Initialization** (SC5, Page 19) | | | | |
|---|---|---|---|---|
| **Requirements from mission and sensors** | **Required Hardware (on SC)** | **Estimated Accuracy and Performance** | **Advantages, Benefits** | **Disadvantages** |
| • Optic with 10-20 mm focal length<br>• Landing from near side<br>• DEM from orbiter necessary<br>• Rotation around z less than 10 degrees | • camera (500x500 pixels)<br>• DSP board<br>• 10 MB memory, | • First position after 10-20 seconds<br>• From 5 km: Errors below 10m in x and y, below 3 m in z | • Allows absolute navigation with respect to global DEM<br>• Very accurate in z<br>• Serves as starting point for tracking and landing on predefined spot<br>• Flexible in terms of image acquisition timing | • Illumination must be similar as for DEM generation from orbit<br>• Bright areas should be well distributed across view |

| **3D Position Update** (SC6, Page 21) | | | | |
|---|---|---|---|---|
| **Requirements from mission and sensors** | **Required Hardware (on SC)** | **Estimated Accuracy and Performance** | **Advantages, Benefits** | **Disadvantages** |
| • Camera pointing accuracy 2 degrees<br>• Optic with 10-20 mm focal length<br>• DEM from orbiter necessary<br>• Position initialization necessary | • camera (500x500 pixels)<br>• DSP board<br>• 8 MB memory, | • Update rate below 10 seconds<br>• Errors in the range of the position initialization; estimated below 20 m for 40 positions | • Seems to be convergent<br>• Flexible in terms of image acquisition rate<br>• Can be used to refine ground distance measurement | • Large shadow areas cannot be crossed<br>• Overlap between subsequent images should be more than 80 % |

| **2D Lateral Motion** Evaluation (SC7, Page 23) | | | | |
|---|---|---|---|---|
| **Requirements from mission and sensors** | **Required Hardware (on SC)** | **Estimated Accuracy and Performance** | **Advantages, Benefits** | **Disadvantages** |
| • Camera pointing accuracy 2 degrees<br>• Optic with 10-20 mm focal length<br>• One accurate narrow angle distance measurement, registered to camera | • camera (500x500 pixels)<br>• DSP board<br>• 8 MB memory, | • Update rate below 10 seconds<br>• Errors per measurement below 1 % of range | • Not dependent on orbiter DEM<br>• No calibration necessary<br>• Horizontal velocity can be measured without accurate distance sensor<br>• Changes in pointing direction can be also measured | • Overlap between subsequent images should be more than 80 %<br>• Necessity of narrow angle distance measurement |

| **2D Obstacle Detection** (SC8, Page 24) | | | | |
|---|---|---|---|---|
| **Requirements from mission and sensors** | **Required Hardware (on SC)** | **Estimated Accuracy and Performance** | **Advantages, Benefits** | **Disadvantages** |
| • Optic with 10-20 mm focal length<br>• Rough distance estimate | • camera (500x500 pixels)<br>• DSP board<br>• 4 MB memory, | • Update rate below 2 seconds<br>• 95% detection of obstacles below 1 m from 100 m distance | • No calibration necessary<br>• Applicable also from larger distances for 2D based slope detection<br>• Fast | • Parameters must be adjusted to estimated terrain roughness / obstacle distribution |

These components were used for the definition of two target strategies. The first strategy is a minimal vision tool that can be used for 2D obstacle detection and safe landing site selection during late descent. The second strategy enables full 3D navigation and a closed-loop landing

Experiments show that the closed-loop navigation accuracy is in the range of 10 m. In a specific simulation using real images and a mockup scaled linearly by a factor of 1:3000 the position errors as result of the DEM stereo reconstruction - position initialization - tracking obtained less than 3 m error in all three directions.

A large set of experiments evaluated important parameters in terms of sensing, accuracy, error behavior, robustness and influence of environmental conditions to specific strategy components as well as complex processing chains. The major results of these experiments and theoretical analysis are listed below:

- **The expected RMS disparity error is 0.4 pixels for realistic configurations.**
- **The expected disparity error of 0.4 pixels does not heavily contribute to DEM generation errors compared to calibration errors. The expected error is about 2 meters (elevation) using a typical sensor with 100 mm focal length (option C), 25 km ground distance and 30 degrees base angle.**
- **A DEM stereo reconstruction error of 6-7 meters (RMS in z) can be extrapolated from mockup experiments.**
- **For lander navigation using a DEM from orbit, the usage of a wide angle lens is preferred, since the influence of errors in 3D positions on the DEM is worse for narrow angle lenses.**
- **Expected position errors in x and y are about the same as the 3D landmark point errors. Errors in z are 1/5 of the 3D point error on the DEM.**
- **Three different investigated orbiter sensor options (between 100 and 200 mm focal length) allow a self-calibration accuracy of less than 10 meters.**
- **The errors of self-calibration for the lander motion stereo case are not significant in comparison with the reconstruction errors.**
- **The expected position initialization error using a 3m resolution DEM and an optical sensor with 700x500 pixels (focal length = 14mm) will be below 10 meters in x and y, and below 3 meters in z.**
- **Tracking does not become unstable even if the first position suffers from a relatively high error**.
- **The number of images used for tracking is not a crucial parameter (numbers up to 200 positions were investigated) and the pointing noise can be up to +/- 2 Gon.**
- **The optimum number of landmarks is at about 500 points, backprojection threshold is not a crucial factor for tracking. However, a smaller set of landmarks (>200) still leads to robust tracking**

- **Unlike tracking, the lateral motion measurement without reference DEM should be performed with update frequency as low as possible.**
- **A detection rate of 95 % for 60-100cm obstacles from 100 m distance and a detection rate of 80-90 % for 1-1.5m obstacles from 250 m distance could be found for the 2D obstacle detection algorithm (lander sensor with 14mm focal length)**
- **At the last position of a real closed-loop simulation, a navigation error of less than 1 mm (corresponding to 3 m in reality) was achieved.**
-

**All those results show that under the identified valid conditions the application of computer vision for supporting an unmanned landing on the Lunar surface does make sense. Fully autonomous landing using the vision algorithms introduced is feasible with the required accuracy.**

**The vision approach as solution for supporting a safe and accurate landing as major decision component is promising enough to continue with more detailed studies and explicit realistic experiments.**

# 13 BIBLIOGRAPHY

## References

[Bau94] Arnold Bauer. Stereo Reconstruction from Dense Disparity Maps Using the Locus Method. Master's thesis, Technische Universität Graz, 1994. Diplomarbeit.

[Mat93] Matra Marconi. Autonomous and Advanced Navigation Techniques. Executive Summary of ESTEC contract 8808/90/NL/PM/SC, ESA, Nordwijk, April 1993.

[Par94] S.M. Parkes. Vision Lander PBMT1: Flight model definition, real time processor definition. Wp 21 report, British Aerospace Systems Ltd., Nordwijk, July 1994.

[PPC92] Paar, G., Pölzleitner, W., and Classen, H.J. Planetary High Resolution Model of Terrain. Final Report of ESTEC contract 9195/90/NL/SF, Joanneum Research, CAE, Nordwijk, November 1992.

[PSC+94] Paar, G., Sidla, O., Classen, H.-J., Parkes, S.M., and Gillions, A. Planetary Body High Resolution 3D Modeling, phase 1 report. Technical report, European Space Research and Technology Centre, Noordwijk, The Netherlands, February 1994.

# 14 APPENDIX A

## A Error Estimation

### A.1 Preliminary Considerations

In this section we consider the theoretical background of the error estimations used. We have the following problem.

Let $f(x,p)$ be a smooth, positive function of the variable vector $x \in \mathbf{R}^n$ and the parameter vaector $p \in \mathbf{R}^m$ with values in $\mathbf{R}$. For a given parameter vector $p$ we are interested in the vector $x(p)$ that satisfies

$$f(x(p),p) = \min_{y \in \mathbf{R}^n} f(y,p). \tag{1}$$

We now want to examine the expected value $\mu_{x_i}$ and the standard deviation $\sigma_{x_i}$ of the components $x_i$ of $x(p)$ for a given probability distribution of $p$.

Additionally, we assume the following scenario. For a certain parameter vector $p_0$ and a certain variable vector $x_0 = x(p_0)$, we get $f(x_0,p_0) = 0$, and for all $p \neq p_0$ and all $x \neq x_0$, we get $f(x,p) > 0$.

Without loss of generality we can assume that $p_0 = 0$, and $x_0 = 0$. Furthermore we know that $f(0,0) = 0$, $f_{x_i}(0,0) = 0$ for all $i = 1 \cdots n$, and $f_{p_j}(0,0) = 0$ for all $j = 1 \cdots m$. We can now approximate f by the first terms of its Taylor series.

$$f(x,p) \approx x^T A x + x^T B p + p^T C p, \tag{2}$$

where $A = \left(f_{x_i x_j}(0,0)\right)$, $B = \left(f_{x_i p_j}(0,0)\right)$, and $C = \left(f_{p_i p_j}(0,0)\right)$.

From the condition $f_{x_i}(x(p),p) = 0$ and equation (2) we obtain

$$x(p) = -\frac{1}{2} A^{-1} B p. \tag{3}$$

For convenience we set $M = -\frac{1}{2} A^{-1} B$. It is now easy to see that

$$\mu_{x_i} = \sum_{j=1}^{m} M_{ij}\, \mu(p_j) \tag{4}$$

and

$$\sigma_{x_i}^2 = \sum_{j=1}^{m} M_{ij}^2\, \sigma(p_j)^2. \tag{5}$$

Next, we describe how our particular problems fit into this abstract setting.

### A.2 Absolute Calibration

For the absolute calibration we take as variables the extrinsic parameters (the translation vector $t$ and the angles $\omega$, $\phi$, and $\kappa$ which define the rotation matrix $R$). We take as parameters the image coordinates $(u_i, v_i)$, and the world